Climate Dynamics
https://doi.org/10.1007/s00382-019-05040-4

Future changes in Atlantic hurricanes with the rotated-stretched ARPEGE-Climat at very high resolution

Fabrice Chauvin[1] · **Romain Pilon**[2] · **Philippe Palany**[2] · **Ali Belmadani**[2]

Received: 25 March 2019 / Accepted: 31 October 2019

Abstract
The new CNRM-CM6 release of the CNRM/CERFACS atmospheric general circulation model has been used in a rotated/stretched configuration that allows a local horizontal resolution of less than 15 km over the tropical North Atlantic basin. Sea surface temperatures (SST) arise from a previous lower resolution simulation of the Coupled Model Intercomparison Project-5 exercise and corrected through a quantile–quantile method. Moreover, five-member ensemble simulations have been performed for both present and RCP8.5 scenario climates. For validation purposes, another five-member ensemble simulation has been performed with prescribed observed SST. Tracking of tropical cyclones (TCs) in these simulations reveals that the intensity of the simulated TCs are quite realistic and may reach the strongest hurricane ever observed, allowing to distinguish between TC categories in the analysis. Although the model tends to underestimate the occurrence of TCs over low latitudes, the realism of simulated TCs has nevertheless improved compared to previous versions of the model, due to both increased resolution and changes in the parameterizations used in the model. Changes observed in the simulations between present and future climates confirm previous results stating that there is no clear change in the overall number of TCs but an increase in the intensity of major hurricanes as well as an increase of rainfall in all TC categories. A new result suggests that TC activity response to climate warming may be significantly different from 1 month of the hurricane season to another. In our simulations we observe a robust decrease of TCs in the tropics in July while August and September experience a large increase of TCs over the mid-latitudes. Finally, we find a relation between a large increase in TC activity near the African coast and changes in the African atmospheric dynamics and rainfall in September.

1 Introduction

TCs are the deadliest and costliest meteorological phenomena in the world if one refers to the "Atlas of mortality and economic losses from weather, climate and water extremes 1970–2012" (WMO 2014). The 2017 Atlantic TC season has been one of the most active seasons after 2005 and Irma, which lasted from August 30th to September 12th, accounted for at least one-third of the total seasonal Accumulated Cyclone Energy (ACE), which is calculated from the integrated 6-hourly maximum wind speed along the lifetime of the named tropical storms and accumulated over the hurricane season. While the environmental conditions necessary for TC formation have been relatively well known since the works of Gray (1968, 1975), the complete representation of TCs in global climate models (GCMs) remains a difficult challenge due to the multi-scale nature of these phenomena. Early attempts to simulate TCs have emphasized the necessity of parameterizing convective processes to account for realistic representation of TCs in the models (Ooyama 1982). As early as 1969, Ooyama demonstrated that it was possible to simulate an axisymmetric, quasi-balanced vortex in a stable stratified incompressible fluid (Ooyama 1969).

Climatic assessment of TCs and more specifically, the impact of anthropogenic global warming still suffers from the coarse resolution of the coupled atmosphere–ocean general circulation models (AOGCM) to represent TC-like vortices that can reach TC intensities. In the framework

Electronic supplementary material The online version of this article (https://doi.org/10.1007/s00382-019-05040-4) contains supplementary material, which is available to authorized users.

✉ Fabrice Chauvin
fabrice.chauvin@meteo.fr

[1] Centre National de Recherches Météorologiques, Météo-France/CNRS, Météo-France 42 avenue G. Coriolis, 31057 Toulouse Cedex 1, France

[2] Direction InterRégionale Antilles-Guyane, Météo-France, Fort-de-France, France

Published online: 14 November 2019

of the Coupled Model Intercomparison Project (CMIP), increasing resolution is a slow process owing to the difficulty of maintaining fully coupled AOGCMs and to perform long simulations. At climate scales, models are generally considered high-resolved for horizontal grid scale less than 50 km, even though some climate centers now reach around 20 km globally (Oouchi et al. 2006). At 50 km resolution, TC characteristics are relatively well represented (among them a warm core and maximum tangential wind at the lowest levels) but their intensity is generally underestimated (Walsh et al. 2007). Dynamical downscaling with limited area models (LAMs) presents the advantage of increasing the resolution and thus the realism of modeled TCs. Nevertheless, these models must be constrained at their boundaries, which is a source of uncertainty since coherency between local and remote climate is not necessarily obvious.

According to the last Intergovernmental Panel on Climate Change (IPCC) report (Stocker et al. 2013) and subsequent studies, there are still some uncertainties in the response of TCs to climate warming (Royer and Chauvin 2009; Knutson et al. 2010, 2013, 2015; Murakami et al. 2012a; Emanuel 2013, 2015; Kossin et al. 2014; Walsh et al. 2016; Bhatia et al. 2018). One among other reasons for this is that most models used in CMIP5 cannot directly address TC activity due to their coarse resolution although a few of them can do it (Bengtsson et al. 2007; Murakami et al. 2012b; Oouchi et al. 2006; Sugi et al. 2009; Yamada et al. 2010; Zhao et al. 2009). Low resolution models can nevertheless provide some insight through cyclogenesis indices, which are combinations of large-scale climate variables favorable for TC genesis. This approach has been introduced in the 70s by Gray (1968, 1975) and widely investigated during the last 30 years (Royer et al. 1998; McDonald et al. 2005; Camargo et al. 2007; Emanuel and Nolan 2004; Menkes et al. 2012). Through combinations of these environmental conditions (generally at the monthly or seasonal timescale), genesis indices may be constructed to reproduce the probability of cyclogenesis (or more generally TC activity, given that conditions that favor cyclogenesis also favor mature stages) and thus study changes in this probability under different forcing conditions. One of the first attempts to address the global warming effect on TC genesis was done by Royer et al. (1998), who introduced the convective yearly genesis parameter (CYGP) based on the yearly genesis parameter (YGP) of Gray (1975) but where all the thermal component had been replaced by the convective precipitation diagnosed in the model. Indeed, the YGP could not be used for climate change studies due to the included use of a 26 °C sea surface temperature (SST) threshold, which may not be relevant in a changed climate. Camargo et al. (2007) have demonstrated the ability of the Genesis Potential Index (GPI) of Emanuel and Nolan (2004) to reproduce both the annual cycle of TC activity and the impact of the El Nino–Southern Oscillation (ENSO) on TC genesis. However, Menkes et al. (2012) highlighted the difficulties to reproduce the remaining interannual variability of TC activity.

Although cyclogenesis indices have shown their usefulness for seasonal and some limited interannual time-scales, the response of these indices to climate warming is highly uncertain (Royer and Chauvin 2009). High-resolution models, which allow a direct counting of TCs, indicate however that the global number of TCs may remain stable or slightly decrease with the increase in global temperature (see Fig. 14.17 of Stocker et al. 2013). Is the discrepancy between the two approaches due to drawbacks in cyclogenesis indices or just to limited number of high-resolution simulations taken into account? The response might probably emerge from the new CMIP6 exercise, which will include the HighResMip project (Haarsma et al. 2016). Indeed, this project aims at enabling an intercomparison between several high resolution models run under a common protocol. The target of the project is to understand the impact of the resolution on the simulations of high risk events, with a particular focus on tropical cyclones. Nevertheless, it remains interesting to continue investigating the cyclogenesis indices approach since it allows to address the very large multi-ensemble database of low-resolution model simulations, while we would still have to wait a long time before getting such a large ensemble for high-resolution model simulations.

At the Centre National de Recherches Météorologiques (CNRM), the research center of the French national weather service (Météo-France), an original configuration of the ARPEGE-Climat model allows focusing on a specific region while keeping a global approach through the ability to stretch and rotate the grid of the model. This configuration, also used operationally for meteorological forecasts, has been widely used in previous TC studies (Chauvin et al. 2006, 2017; Daloz et al. 2012). In the frame of the new CMIP6 project, the atmospheric and land-surface components of the CNRM-CM model have been largely modified since CMIP5. Moreover, with the increased computation allocations, it is now possible to run high resolution models for long periods. The stretching technique adds a supplementary improvement since resolutions equivalent to limited area models (LAM) are now reachable. It is thus natural to investigate the response of TCs to anthropogenic warming with such a configuration without the drawbacks of the boundary condition problems of LAMs.

The paper is organized as follows. Section 2 introduces the model, the experimental design, and the tracking method used in this study. Section 3 assesses the performance of the present simulations compared to observations. Effects of climate warming on TCs are presented in Sect. 4. Finally, a summary and a conclusion are given in Sect. 5.

2 Experimental design

The new CNRM-CM6 version of the Météo-France AOGCM has been developed during the past few years in order to participate in the future CMIP6. The land–atmosphere model involves the ARPEGE atmospheric GCM and the SURFEX land surface model (Masson et al. 2013). The version used here was frozen in a quasi-final version of the atmospheric component of the global system that will be used for the coming CMIP6 exercise.

The ARPEGE model has the particular ability to allow a deformation of its horizontal grid so as to focus on a region of interest. To do so, the pole of the grid is rotated over the center of this region. Then, a stretching factor is applied in order to locally increase the resolution at the expense of the antipode. Thus, for the cost of a uniform low-resolution simulation, one can obtain a locally high-resolution simulation without the lateral boundary problem that arises in LAMs. Variable resolution have been used at Météo-France (MF) since the 90s. In our knowledge MF was the first National Weather Service to introduce this refinement in the operational models (Courtier and Geleyn 1988; Yessad and Bénard 1996). Since then, this configuration have been largely used in climate studies (Déqué and Piedelievre 1995; Lorant and Royer 2001; Gibelin and Déqué 2003; Fox-Rabinovitz et al. 2006) and particularly in TCs dedicated climate studies at MF (Chauvin et al. 2006, 2017; Daloz et al. 2012). In Chauvin et al. (2006), the authors validated the variable-resolution configuration for TC climate studies. They compared changes of TCs with warming between the variable-resolution and corresponding uniform resolution and found that the response was mainly identical at the basin scale over the Atlantic. Moreover, they also emphasized that the SST change pattern by wich the model was forced explained most of the differences between different runs. Daloz et al. (2012) identified that the position of the high-resolution pole had and impact on the TC density by comparing two 50-years long simulations, one with the pole near the Africa coast and the other in the middle of the Atlantic, at the same place as in the present study. The latter did produce the best estimation of the TC density. The other run exaggerated the eastern Atlantic TC activity while largely missing the Gulf of Mexico (GoM) and Florida ones.

Considerable effort has been made since the CNRM-CM5 version by the development team of MF in order to improve the quality of the model. Among the various developments, the implementation of the new physical package Prognostic Condensates Microphysics and Transport (PCMT), which involves a new convection scheme (Piriou et al. 2007; Gueremy 2011) and some new prognostic variables (such as liquid and ice water), represented a large contribution to global efforts of the team (Voldoire et al. 2019). A new micro-physics scheme (Lopez 2002) and a new turbulence scheme based on eddy kinetic energy (Cuxart et al. 2000) have also been implemented. The new convective scheme is a mass-fluss based prognostic scheme which allows a unified approach of the dry, shallow and deep convection. The closure of the scheme is based on CAPE relaxation and a prognostic equation is introduced for the vertical velocity in the updrafts which is used for the triggering condition. Additionally, prognostic equations have been introduced for the different phases of the liquid and solid water which allows the use of the same microphysics for convective and resolved part of these variables. A resolution dependency is introduced in the scheme to ensure that rainfall produced by the convection over a fixed area is not dependent on resolution. In other words, as grid size decreases, the convective grid fraction must increase to account for the real size of convective systems. This is particularly relevant for variable resolution since the local mapping factor can reach the mean resolution multiplied (resp. divided) by the stretching factor (here 3.5) at the highest (resp. lowest) resolution. The resolution dependency is assumed via the convective response time which is the time required for the CAPE to be reduced to zero by convective processes in the absence of large scale forcings. Convective fraction depends on this response time.

In our set of experiments, the pole was located at 20° N and 50° W, with a stretching factor of 3.5 applied to a T359 linear grid, resulting in a local resolution of T1256 in the center of the tropical North Atlantic. This corresponds to a maximum equivalent spatial resolution of ~ 14 km. Figure 1 shows the representation of the equivalent grid sizes expressed in kilometers. Over the North Atlantic Ocean basin, horizontal resolution ranges between 14 and 30 km over the active TC region except the GoM whose resolution is around 35 km. The time step is 600 s in all the runs and 6-hourly outputs were archived. The version of the model is almost the same (the version was fixed just before the last refinements of the CNRM-CM6 model) as the one that will be used for the set of simulations that CNRM will perform in the frame of the CMIP6 project (Voldoire et al. 2019).

Three 5-member ensemble simulations were performed in order to consider a sufficient number of TC tracks and thereby address the robustness of our results. Members only differ by their initial conditions: 1st of January at different years from a previous run (the same as the following used for surface conditions forcing). The three sets were defined as follows:

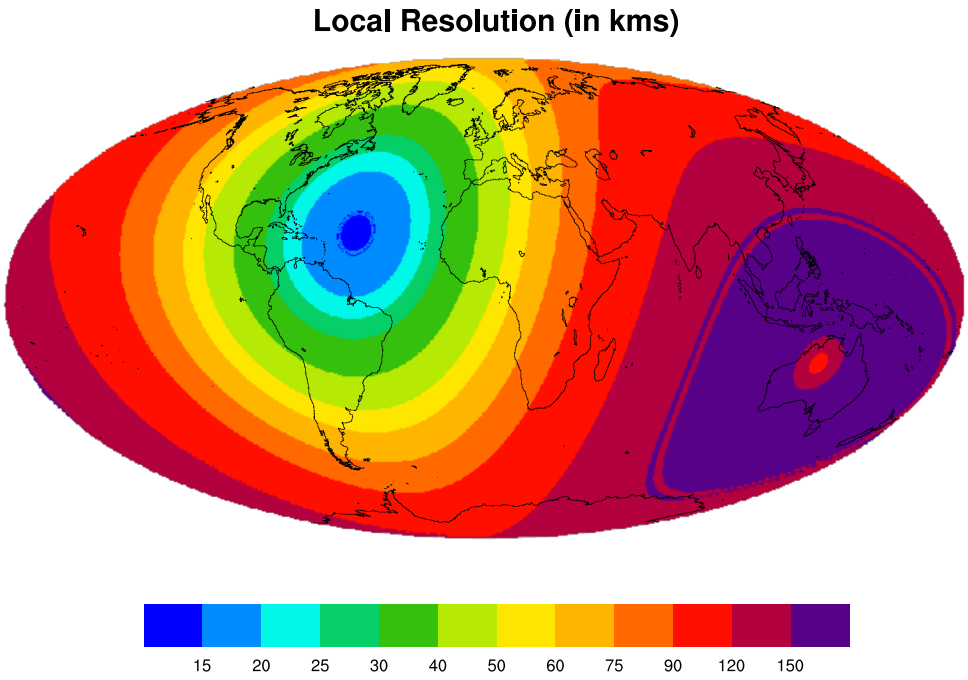

Fig. 1 Equivalent grid representation of the spectral rotated stretched T359grid. Colors correspond to area grid point size expressed as the length of one of the sides of the corresponding square (in km)

- one set of simulations with prescribed SST and sea-ice concentration (SIC) from Hadisst1 dataset (WMO 2014), referred hereafter as AMIP-Obs;
- one set of simulations with prescribed SST and SIC from one of the historical simulations performed with the CNRM-CM5 model for the CMIP5 exercise (Voldoire et al. 2013), and previously corrected as described below, referred hereafter as AMIP-Hist;
- one set of simulations with prescribed corrected SST and SIC from a RCP8.5 scenario performed with the same model, referred hereafter as AMIP-RCP85.

The periods covered by the simulations are 1965–2014, 1965–2013 and 2031–2080 for the AMIP-obs, the AMIP-historical and the AMIP-RCP85 runs, respectively.

This experimental design was determined so that we could (1) validate the simulated TCs with observations using the runs constrained by observed SSTs (AMIP-Obs), and (2) measure the evolution of TCs between present (AMIP-Hist) and future climates (AMIP-RCP85).

2.1 SST and SIC prescribing

All the simulations presented here were performed in Atmospheric Model Intercomparison Project (AMIP)-type mode, with prescribed SSTs and SIC from either observations (Hadisst1) or CNRM-CM5 historical or RCP8.5 scenarios. Prescribed model SST and SIC were corrected to ensure unbiased climatological means as described further in the next section.

2.1.1 Quantile SST and SIC correction method

In this paper, the authors present the methodology used to correct the modeled historical SSTs toward the observed ones but also suggest a method to correct the SSTs from future scenarii considering the historical ones. The methodology used to correct SSTs follows (Li et al. 2010).

For the AMIP-Hist runs a direct quantile–quantile correction was applied. For each model ocean grid point, each monthly mean SST was identified by its quantile in the cumulative distribution function (CDF) of all the SSTs encountered for this particular grid point. The corresponding SST quantile in the AMIP-Obs runs was then attributed to this grid point for this particular month. The resulting CDF for the corrected SST thus corresponds exactly to the CDF of observed SST. For the future runs, a slightly different correction is applied in order to consider the shift in the CDF due to climate warming. For each ocean grid point and for each month of the future simulations, the corresponding quantile is compared with the quantile in the present CDF and the difference is added to the observed CDF in order to obtain the corrected future SST. The resulting future CDF is nothing else than the sum of the observed CDF and the future minus present CDF.

For the correction of SIC, a direct quantile–quantile correction did not appear to us as a good approach since the SIC variable is constrained between two constant values of 0 and 100%. It would be problematic to establish a transfer function between observed and modeled SIC since the CDF have constant values of 0 or 1 for a large part of the gridpoints. We adopted a method described by Haarsma et al. (2016).

The CDF of the observed SST is partitioned with 0.1 °C binwidth and the mean observed SIC is calculated for each of the intervals. The resulting observed transfer function is assumed to be identical for observed and corrected modeled SSTs so that it can be applied to the latter without any further correction. Notice that for future particularly warm SSTs that may not have been encountered in the present simulations, the SIC is attributed the value associated with the highest SST bin encountered at the corresponding gridpoint. Haarsma et al. (2016) nevertheless recommend to differentiate between Arctic and Antarctic regions to construct the transfer functions since the SST/SIC relationship may differ between the two regions. We adopted their recommendations in our study.

2.1.2 Conserving the monthly means

When prescribing monthly SST and SIC for atmospheric model simulations, they are generally linearly interpolated at the daily timescale according to the position of the day in the month. However, this operation does not conserve the initial monthly means and may introduce non negligible biases. As recommended in the AMIP experimental protocol (Taylor et al. 2000), we applied the Program for Climate Model Diagnosis and Intercomparison (PCMDI) program, which calculates the prescribed SST and SIC so that monthly means of daily interpolated variables are those of the initial dataset.

2.2 Tracking algorithm

TCs are objectively tracked in the simulations with an algorithm described in details by Chauvin et al. (2006). Appropriate threshold values adopted in this study have been adapted to the model characteristics and resolution, while the core of the TC tracking algorithm has been conserved. Indeed, since the meteorological fields are projected on a 15 km regular grid before tracking, some of the thresholds convenient for 50 km projections in previous studies were not accurate. Moreover, the tracking uses a quality parameter relative to the displacement of the TC that have to be adapted to the 15 km grid. TCs are detected when the 850 hPa local vorticity is above a threshold and the mean sea level pressure is at a minimum. Additional conditions are as follows: 10-m wind (> 17 ms^{-1}), warm core and strongest winds at lower levels. All these conditions are expected to differentiate TCs from other atmospheric perturbations.

Once TC centers have been detected, tracks are constructed from their successive 6-hourly positions by following a best quality selection criteria. One of these criteria takes into account the distance of the selected maximum to the expected geometrical position. When two maxima are in competition to complete a track at time $t+1$, one selects the local maximum which is the closest to the position extrapolated from the $[t-1, t]$ segment.

Finally, for track-counting applications, a completing track algorithm is used. Each track is completed by relaxing all the criteria except the vorticity threshold. The track can thus be completed backward from its beginning and forward after its ending point. Moreover, tracks can be completed within the life cycle of the TC when one or more of the criteria are no more fulfilled, which would otherwise lead to a double track counting for the same TC.

3 Validation of the simulations

Simulated TCs in the AMIP-Obs are compared with the IBTrACS dataset (Knapp et al. 2010) over the same 1965–2014 period.

3.1 TC intensities

Figure 2 shows the scatter plot of lifetime minimum sea level pressure (P_{min}) versus maximum 10-m wind intensity (V_{max}) for IBTracs (black), the first member of the AMIP-Obs experiment (blue) and two additional runs for comparison: a CNRM-CM5 simulation in T127 variable resolution (green, Daloz et al. 2012) and a T359 uniform resolution

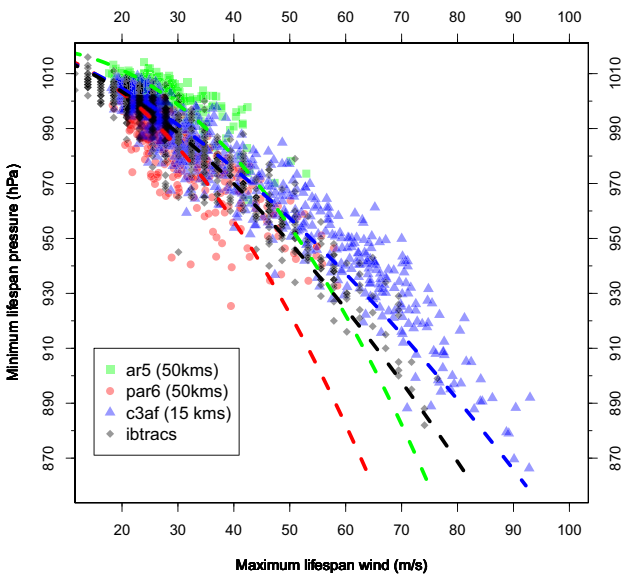

Fig. 2 Scatter plot of lifetime minimum sea level pressure (hPa) versus maximum 10 m wind intensity (ms^{-1}). Black diamonds correspond to IBTrACS TCs (one diamond per TC) and black curve represents the empirical relationship calculated following Atkinson and Holliday (1977). Blue triangles are for the first member of AMIP-OBS experiment, forced with observed SSTs. For comparison, a uniform T359 run has been represented as red dots (see text for description) and runs from Daloz et al. (2012) as green squares

simulation with the same model version as AMIP-Obs (red). Each symbol on the figure represents one TC. For each run, an empirical P_{min}/V_{max} relationship has been calculated following Atkinson and Holliday (1977). AOur AMIP-Obs run tend to sligthly overestimate IBTrACS TC intensities. That means that the high resolution of our simulations allows the development of very strong TCs. Indeed, as many as four TCs reach P_{min} lower than the lowest ever recorded in the Atlantic basin, which was 882 hPa for category-5 hurricane Wilma in 2005 (Pasch et al. 2006). This is even more marked for wind intensity since as many as seven TCs are stronger than the 1-min sustained 84.7 ms^{-1} [reported in Fig. 2 as a 10-min sustained wind of 76.3 ms^{-1} according to Powell et al. (1996)] recorded for hurricane Allen in 1980. Part of this overestimation may result from the lack of ocean–atmosphere coupling that tends to reduce TC intensities by the cooling effect feedback (Zarzycki 2016; Li and Sriver 2018). But all changes in parameterizations that have been introduced since the previous version of the model may explain another part of the overestimation of TCs. By comparison, the 50-km simulations (1950–1999) used by Daloz et al. (2012) did not produce TCs with wind exceeding 55 ms^{-1} (green squares in Fig. 2) while the uniform T359 simulation reaches several times 60 ms^{-1} during a smaller period (1979–2010). Thus, the very strong intensities seen in the AMIP-Obs simulation are a combination of model parameterization, lack of coupling and high resolution.

Another striking point is the similarity between the empirical relationships calculated for the model and observations. The black and blue dashed curves lie close to each other, while the slope of the red and green curves are stronger. As suggested by the red dashed curve, V_{max} in the uniform 50 km simulation are smaller than expected from the observed V_{max}/P_{min} empirical relationship,. It should be noted however that the length of the simulation is shorter than in AMIP-Obs and may miss strong TC occurrences.

3.2 TC tracks

Positions of modelled TC tracks is another important point when addressing present and future TC risks. Figure 3 shows IBTrACS and modeled densities of TC days over the Atlantic basin for the months of July, August and September. Calculation of density is described in the "Appendix". The observed TC activity varies among the different months of the hurricane season. During July, activity is mainly located in the GoM and East of the Carolina coast around 30° N. During August the activity spreads northeastward and southeastward with activity beginning inside the MDR. In September, the TC activity peak is reached over the main part of the Atlantic basin. Furthermore, the MDR is largely represented in the overall activity and the extension northward of 40° N is maximum. The model tends to underestimate TC activity over the Main Development Region (MDR), the Caribbean and the GoM. Conversely, subtropical and mid-latitude activity tends to be overestimated in the center of the basin, mostly during July and August.

The MDR underestimation of TC activity has already been diagnosed in the previous versions of the ARPEGE-Climat GCM (Chauvin et al. 2006; Daloz et al. 2012). However, the lack of TCs in these previous versions of the model was not so marked and did not concern the totality of the MDR. The model now incorporates a new cloud parameterization, including a completely different convection scheme. Thus, the underestimation may depend on how subgrid-scale convection is represented but may also be associated with cyclogenesis processes and interactions with the dynamics of African easterly waves (AEWs).

However, one striking feature is the strong underestimation of TC activity over the GoM in September. It may partly be explained by the lack of TC activity over the MDR in the model but it also suggests that too few TCs develop locally, as can be seen on Fig. 4. Indeed, on this figure, one can see that TC genesis is largely underestimated over the GoM during August and September. More generally, TC genesis is underestimated over the regions of observed TCs while overestimated over the mid-latitudes during the 3 months. According to Harris et al. (2016), variable resolution models may produce a spurious Walker circulation in the tropics, leading to displaced zones of TC activity. We did the same diagnostic of the Walker circulation as Harris et al. (2016) and found that our configuration did not differ from an equivalent T359 uniform configuration. Rainfall over the GoM is also quite similar (not shown). This lack of spurious behavior may arise from the scale-aware parameterization of the convection. As mentioned earlier, the spatial resolution over the GoM is lower than in the remaining TC genesis regions and this may be one reason for reduced cyclogenesis even though it is as high as 35 km which is quite reasonable for TC production. Environmental unfavorable conditions may also explain the lack of TC activity. Among those conditions vertical shear of the horizontal wind is one of the most constraining (Vecchi and Soden 2007). Comparisons of the shear over the GoM in our simulations with ERA-Interim and 20CR did not show particular biases that could explain the lack of TC birth in our simulations (not shown). Reasons for this behavior may thus be difficult to address and should be investigated in further studies. The overestimation of TC activity in the subtropics may indicate a tendency for TCs to deviate their tracks early in their lifetime, diminishing the number of TCs that reach the Caribbean. Despite these biases, the model addresses well the increasing activity in August and September as seen in IBTrACS, with maximum activity over the MDR reached in September. In the model, although it has been showed that the southern TC activity was largely underestimated and the northern one

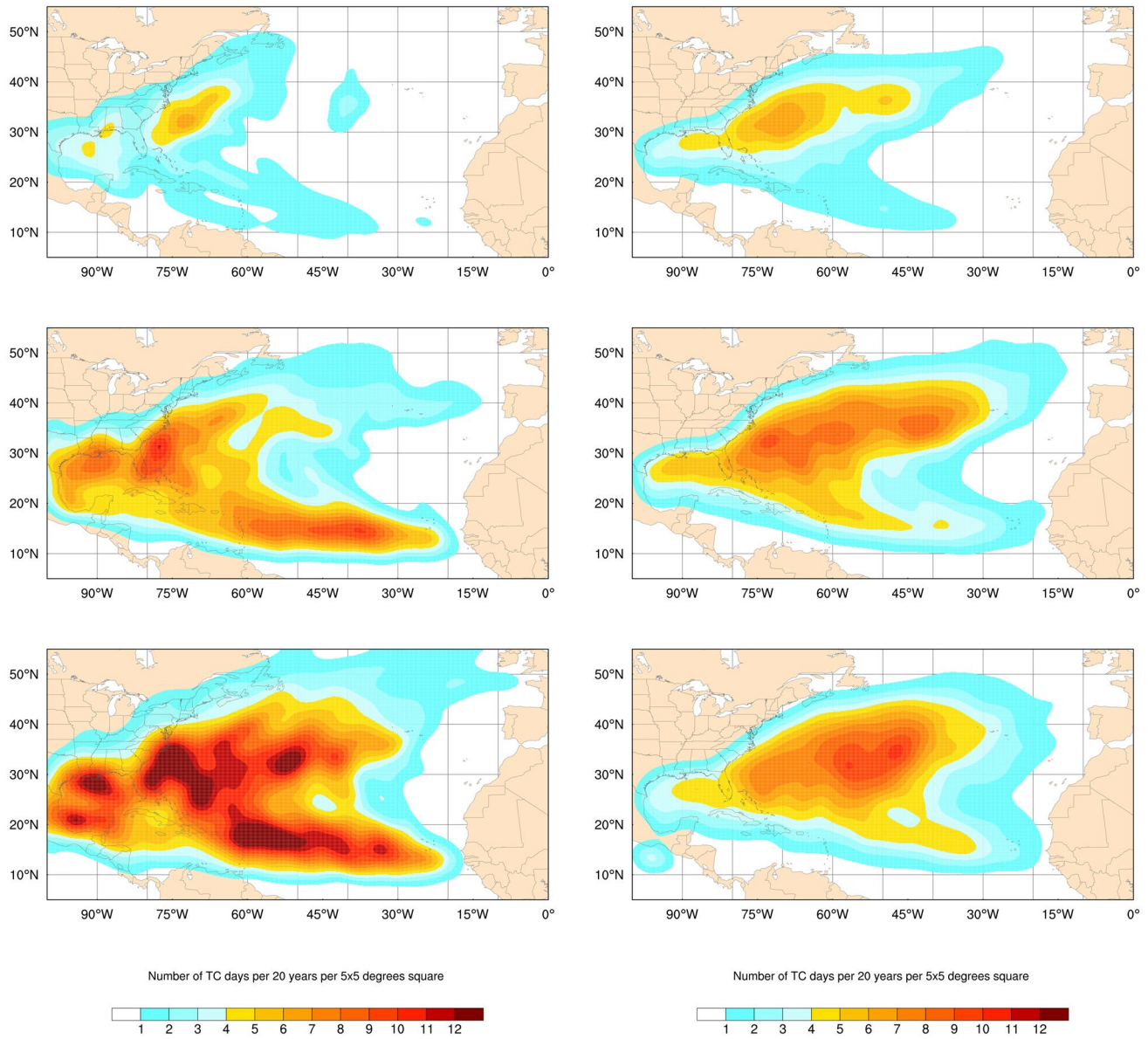

Fig. 3 Observed (IBTrACS) (left side) and modelled (ensemble AMIP-OBS) (right side) TC track days density for months of July (top), August (middle) and September (bottom). Values are expressed as a distance-weighted number of TC days per 20 years by 5°×5° square. A Gaussian diffusion has been applied (see "Appendix" for more details)

overestimated, the annual cycle is fairly well represented. The northeastward extension of TC days density is maximum in August rather than September, suggesting a slight shift in the annual cycle.

3.3 Interannual variability

Since we performed a set of simulations constrained by observed SST and SIC, it is worth addressing the ability of the model to reproduce the interannual variability in TC activity, knowing that a part of this variability is forced by SST anomalies. TC activity over the Atlantic basin is known to be modulated by SST variability at different timescales. The main mode of SST variability acting on the Atlantic TC activity is the ENSO. El Niño (La Niña) years are known to be associated with reduced (enhanced) Atlantic TC activity. According to Camargo et al. (2007) the effects of ENSO on Atlantic TCs are an enhanced vertical wind shear and a reduced mid-tropospheric humidity. SST can also act locally over the Atlantic and influence TC activity. The very active 2005 season and more recently the 2017 season had dramatic effects on the West Indies. They were related to anomalously warm SSTs over the Atlantic basin (Beven et al. 2007). At a longer timescale, the Atlantic multidecadal oscillation

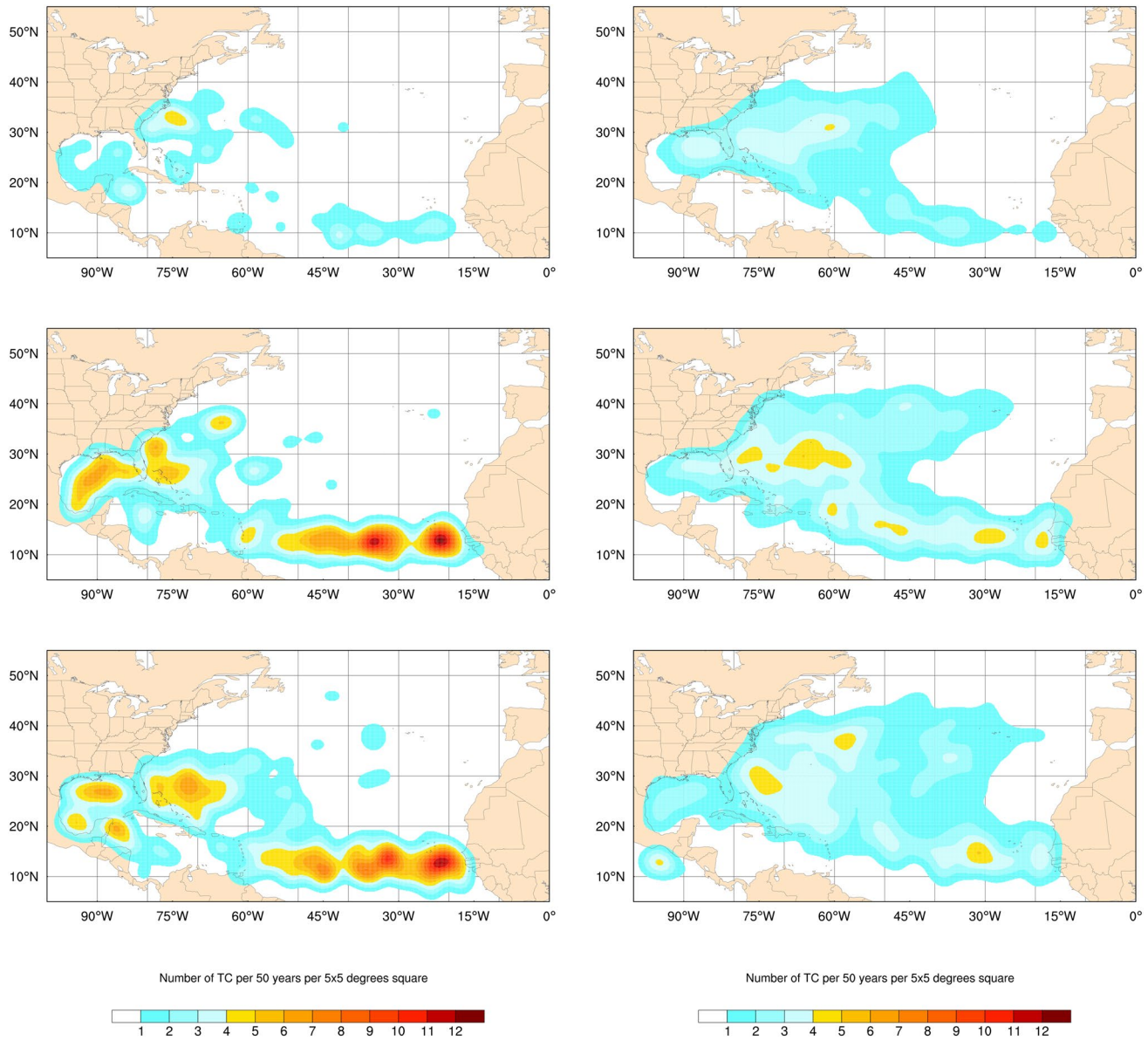

Fig. 4 Same as Fig. 3 but for cyclogenesis densities. Genesis is taken from relaxed tracks with the constraint that 10 m maximum wind intensity is greater than 17 ms^{-1}. Values are expressed as a distance-weighted number of TC birth per 50 years by 5°×5° square. A Gaussian diffusion has been applied (see "Appendix" for more details)

(AMO, Goldenberg and Shapiro 1996) is known to influence the Atlantic TC activity by a modulation of the MDR SSTs (Goldenberg et al. 2001).

All the previous effects have been identified in IBTrACS and one may expect to find the same effects in the AMIP-Obs ensemble. For the AMO, given the shortness of the simulated period, one cannot expect to find a complete cycle in the simulations but at least the reduced TC activity during the 1970–80s followed by an increase during the 1990–2000s detectable in the observations (Goldenberg et al. 2001). Figure 5 shows the interannual variability in the number of TCs in IBTrACS and the AMIP-OBS ensemble runs presented in Sect. 2. Linear trend have been reported for the simulations. It should be noticed that a Student's *t* test has been applied to the trends in the series and none of the trends shown here are significant. We did not report the trend in observations due to uncertainties in the homogeneity of the observed dataset. It is clear however that IBTrACS shows increased activity since the 1990s compared to the two preceding decades, in good accordance with AMO fluctuations (Goldenberg et al. 2001). The model is not able to simulate such a strong modulation even though the period covering 1980–1995 shows a slightly lower activity compared with the remaining periods and corresponds relatively

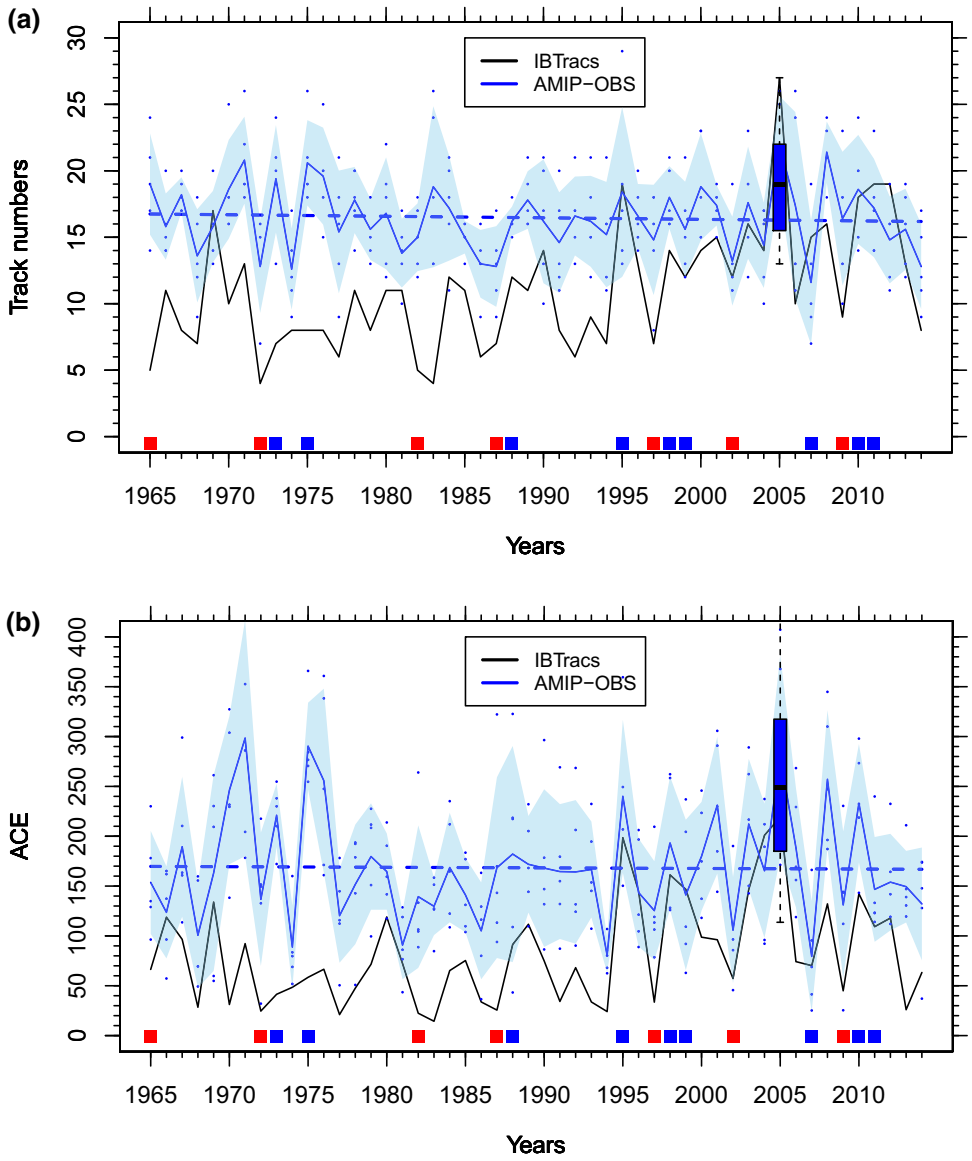

Fig. 5 Interannual variability of **a** number of TCs and **b** ACE in IBTrACS (black) and the AMIP-OBS mean ensemble simulations (blue) over the whole Atlantic basin South of 45 N. Values are the number of tracks per year (top) and $1 \times e^{-4}$ knots^2 for ACE. Shaded light blue area is delimited by the 5-ensemble standard deviation on each side of the mean. The blue boxplot is for the 30-year permanent 2005 run. El Niño (red) and La Niña (blue) years have been reported for the present period as colored squares at the bottom of the figure (see text for details)

well with the observed low activity during this period. Nevertheless, the higher TC activity in the AMIP-Obs (blue curve) ensemble before 1975 is not seen in the IBTrACS dataset nor is phased with AMO fluctuations. Figure 5 also reports the El Niño and La Niña years defined as following. We considered the Oceanic Niño Index, i.e. a 3 month running mean of ERSST.v5 SST anomalies in the Niño 3.4 region (5° N–5° S, 120°–170° W) as calculated by the Climate Prediction Center (https://origin.cpc.ncep.noaa.gov/). If a 3-month anomaly reaches + 1 °C (resp. − 1 °C) during the cyclonic season, the year is considered as an El Niño (resp. La Niña) year. The ability of the model to simulate contrasting TC activity during El Niño and La Niña years is moderate. Indeed, only 4/7 El Niño years (compared with 7/7 years for IBTrACS) lead to below normal TC numbers and 5/9 La Niña years (compared with 5/9 for IBTrACS) lead to above normal TC numbers. For the ACE, results are similar (5/7 versus 7/7 for El Niño years and 5/9 vs. 6/9 for La Niña years). Otherwise, some particularly active years in the observations are fairly well reproduced. This is the case for 1995, 2005 and 2010, which were active years associated with warm MDR anomalies. This behavior is also noticeable in Fig. 5b showing the evolution of the ACE, which may be seen as a more integrated measure of TC activity than only the TC count, as it also takes TC intensity and duration into account. Thus the ability of the model to reproduce the effect of both local SST and remote ENSO on the TC number is moderate and suggests that the relationship between SSTs and TC activity is not simple. As an illustration of this relationship, we investigated more deeply the 2005 year which was a record-breaking year in the observations and which the model showed an ability to simulate

an enhanced TC activity with five-members simulations. Thus, one may expect that the far-above-normal number of observed TC tracks may be simulated in a large ensemble runs. We performed a supplementary dedicated simulation to address this question. A 30-year permanent 2005 simulation was performed and is represented as a blue boxplot in Fig. 5a, b. In Fig. 5a, it can be seen that the dispersion in TC track numbers for 2005 is slightly lower than in AMIP-OBS what is expected due to the size of the sample. However, the mean 2005 TC number is also less than in AMIP-OBS. The maximum encountered TC number in the 30-year simulation does not reach the 2005 observed number. This indicates that the prescribed 2005 SSTs are finally not a strong constraint on the simulated TC number. This may indicate that the model is not enough sensitive to SST anomalies or that the observed breaking-records 2005 TC number was not SST-driven. Presumably, some stochastic effects may partly explain the exceptional TC number in 2005. Indeed, internal variability over the Atlantic has been found to be at least 40% in Done et al. (2014). Their study focused on the 1998 year but may be extrapolated to 2005 since the 2 years exhibited highest than normal TC activity. The major difference, however between the 2 years is that 1998 was a LaNiña year and TC activity may have been partly forced by an externally-driven expected low shear (Bell and Chelliah 2006). Jourdain et al. (2011) also emphasized the highly stochastic nature of TCs in the Southwestern part of the Pacific ocean. They showed that half the variability of TCs here were of stochastic nature. The model, however, reproduces well the observed ACE in 2005 (Fig. 5b). This is probably a result of the model's ability to realistically simulate TC wind intensities. Thus, ACE may be a better index of TC activity than TC number in the model due to the stochastic nature of the TCs. However, if the overall TC activity of the observed 2005 season seems to be partly explained by SST anomalies, the exceptional TC number during this year remains unclear.

4 Response of TC activity to an RCP8.5 scenario

4.1 Mean statistics

Historical (AMIP-HIST) and future (AMIP-RCP85) ensemble runs (green and red curves, respectively) are reported on Fig. 6. Although the trends are not significant, some changes in mean activity are nevertheless detectable. The mean number of TCs is reduced in the future. According to Table 1, the reduction is of 1.6 TCs per year (i.e. ~ 10%), which is significant at the 99% level following a t-test on the global means of each ensemble (i.e. interannual variability is not taken into account). However, there is no significant change in ACE. The reduced number of TCs should thus be compensated by an increase in the intensities and/or number of TC days. This is true for the mean annual maximum wind intensities (maximum wind speed at each time step), which shows an increase of 2.2 ms^{-1} (i.e. 3%) and the mean annual minimum pressure, which shows a 4.1 hPa decrease in the future. These two changes are both significant at the 95% level. Moreover, Table 1 shows the changes in TCs, major TCs and what we have called very strong TCs (VSTCs with a V_{max} greater than 80 ms^{-1}) since the model tends to simulate stronger TCs than observed. As TC number decreases in the future, major TCs do not change but very strong TCs significantly increase (99% level). Table 1 also give statistics for the T359 uniform simulation. It can be seen that at a 50 km resolution, the model can produce hurricanes in a fairly good proportion compared with tropical storms (37%) but misses completely major hurricanes with only 5% of the total systems. The AMIP-Hist five-member simulation produces hurricanes in a proportion of 55% compared with the total systems, which is higher than observation (44% over the period 1965–2014 in IBTracs). Major hurricanes represent 27% of the total systems which is also higher than observation (15%). Thus, at the resolution that we reach with the variable-resolution, the model produces too much and too strong TCs compared with observation.

On average, these results show a modest change with warming climate. Nevertheless, these changes affect the highest side of the intensity distribution, as seen on Fig. 7 showing the relationship between the minimum pressure and the maximum velocity for the AMIP-Hist and AMIP-RCP85 runs. Figure 7 is somewhat different from Fig. 2 in that we addressed the ensemble runs. For clarity of the figure, we plotted the maximum TC intensity per year for all the members. For this reason, we did not produce the fitted curves as in Fig. 2 since it is not expected that the Atkinson and Holliday (1977) formula is valid at the annual time scale. As shown on Fig. 7, although the general relationship is virtually unchanged, the number of years with a maximum TC windspeed exceeding 80 ms^{-1} are more frequent in the future than in the present simulation. This is confirmed by Table 1 showing that one VSTC occurs every 4 years in average in the present climate while in the future, the change is greater than the present count and leads to one VSTC every 2 years in average. Of course, this results may be due to the overestimated TC intensities in the model. Nevertheless, it confirms that a shift in the TC intensities is predicted by the model given that the overall number decreases while strong TC number increases.

4.1.1 Density of track days and genesis

Changes in TC activity may vary from one location to another owing to different changes in environmental conditions. Figure 8a shows changes in the density of TC days

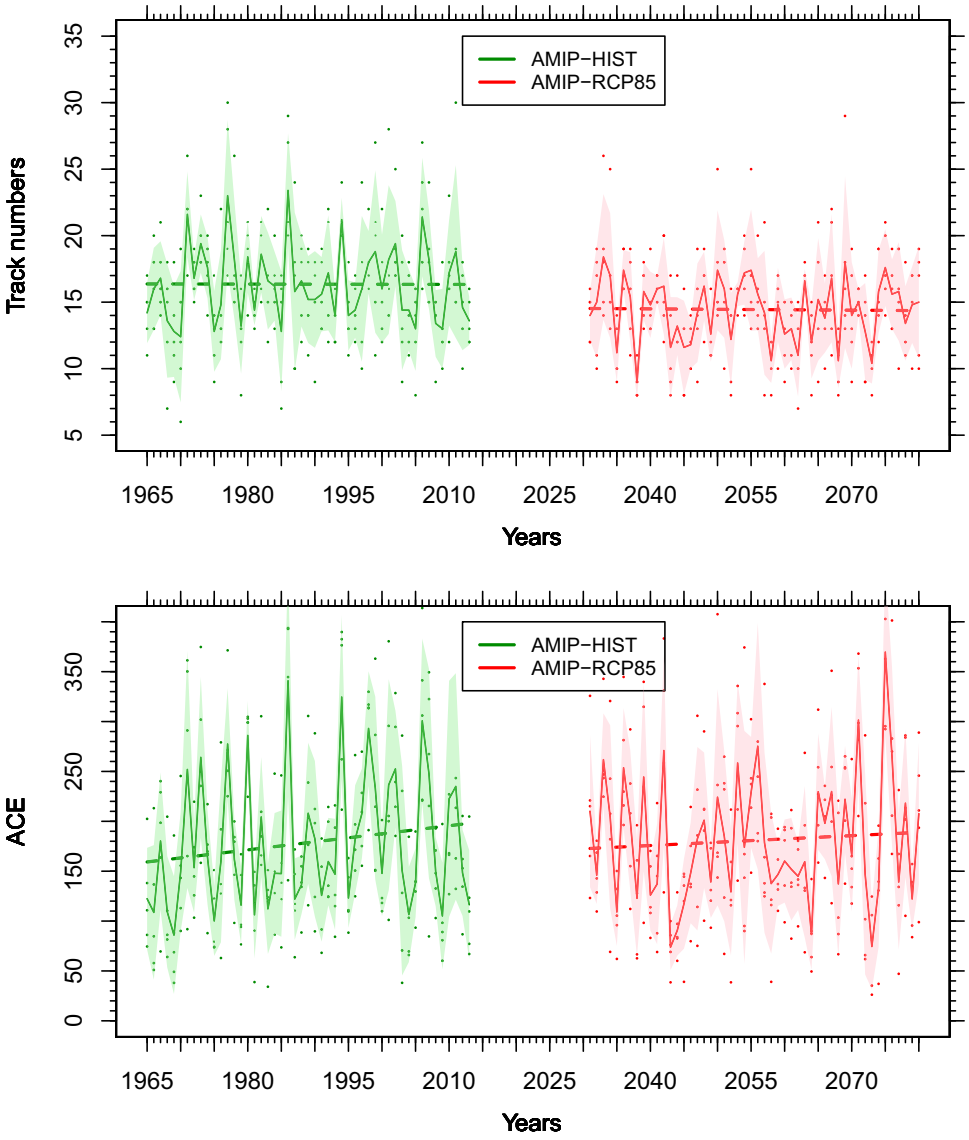

Fig. 6 Same as Fig. 5 for present and future model AMIP-HIST and AMIP-RCP85 ensemble simulations. Data have been plotted following the year of the simulation

Table 1 Future versus present change in some TC characteristics

	AMIP-hist	RCP85 minus hist	Uniform T359
N. storms (per year)	15.8	−1.6**	9.2
N. hurr. (per year)	8.7	−0.6*	3.4
N. major hurr. (per year)	4.2	0.9	0.5
N. very strong hurr. ($V_{max} > 80$ ms^{-1} year^{-1})	0.23	0.21**	0
Mean storm days (days per year)	98.6	−5.9**	51.5
Mean hurr. days (per year)	33.9	−1.2*	9.3
Mean major hurr. days (per year)	15.9	0.8	0.8
Mean very strong hurr. days (per year)	2	3.2**	0
Mean annual V_{max} (ms^{-1})	74.5	1.2	47.1
Mean annual P_{min} (hPa)	913.5	−3.8*	950.1
Mean annual ACE (10^4 knot^2)	204.2	3.8	66.2

Significance levels of the change are 95% (*) and 99% (**). Statistics have been calculated from relaxed tracks to ensure that discontinuous tracks are not counted for several TCs

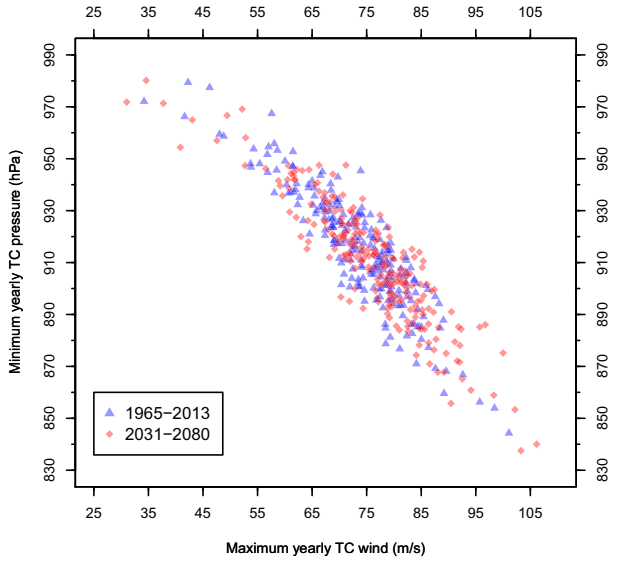

Fig. 7 Scatter plot of yearly minimum TC sea level pressure (hPa) versus maximum TC 10 m wind intensity (ms^{-1}). Blue triangles correspond to first member of AMIP-HIST (one triangle per TC). Red diamonds are for AMIP-RCP85

between present (1965–2013) and future (2031–2080) climates. Figure 8b shows the changes for the cyclogeneses. It was obtained from relaxed tracks, which take into account the days when the system do not fulfill all of the TC criteria and avoids discontinuous tracks to be counted as several systems. Patterns are broadly identical between the two figures, although some details differ mainly due to the fact that cyclogenesis are located upstream of the TC tracks. Most of the patterns are significant at the 95% level due to the low spread between the 5 members of each ensemble. The strongest changes reach a 99% significance level. In our simulations, the number of TC days generally decreases in the future, mainly over the western side of the Atlantic basin, including the GoM and the Caribbean sea, with an extension toward the MDR. The highest reduction (6 days) is located around 30° N. Regional decreases are limited to places such as the GoM or Carolina coast and can reach between 25 and 30% of reduction. Over the West Indies, the reduction is also noticeable in spite of the poor representation of TC density in this region by the model. This reduction is somewhat different from previous studies using the CNRM model. For instance, Chauvin et al. (2006) found a reduction in TC days confined to the GoM and Caribbean regions, with a northeastward increase. They showed that the response pattern was highly dependent on the SST change pattern and on its impact on vertical wind shear. The importance of vertical wind shear for the Atlantic basin was also emphasized by Vecchi and Soden (2007) and Knutson et al. (2013).

Two other regions appear to show some interesting change patterns. The Eastern tropical Atlantic and a region in the mid-latitudes (40°–50° N) see an increase in TC days. The mid-latitude region is located at the boundary of TC activity in the model ensemble simulations. Figure 8a, b suggest a northward extension of TC activity in accordance with previous studies related to the extension of the tropics with climate warming (Staten et al. 2018). Kossin et al. (2014) even demonstrated that the latitude at which TCs reach their maximum intensity has already migrated northward during the last 30 years. This finding confirms past studies such as Murakami and Wang (2010) and Murakami et al. (2012) who found a northeastward shift of TC occurrences in the North Atlantic basin. The other noticeable change concerns the Eastern Atlantic with changes in TC days that exceed 50%. This region extends from the West African coast to approximately 40° W and covers the Cap Verde archipelago, known to be a cyclogenesis region.

4.1.2 Cyclogenesis indices

To explain changes in TC days density, one can look for changes in two cyclogenesis indices combining large scale environment variables: the CYGP (Royer et al. 1998) and the GPI (Emanuel and Nolan 2004). Both genesis indices have some dynamical components in common (shear, vorticity and Coriolis parameter) but differ in their way to take into account the thermal structure of the atmosphere. The GPI thermal component includes the 700 hPa relative humidity, which accounts for mid-troposphere humidity, and potential intensity (Bister and Emanuel 1998), which accounts for temperature and mixing ratio vertical profiles. On the other hand, the CYGP is based on the idea that convective precipitation produced by the model is a good integration of all the previous components by the use of a complex convective-permitting scheme. As seen before, the high spatial resolution used in this study leads to realistic TC intensities. However, strong simulated TC intensities may have an effect on monthly cyclogenesis indices. This is not what is expected from these indices, which have been constructed to account for environmental variables favorable to TC genesis. To ensure that changes in cyclogenesis indices are not due to the TCs themselves, the indices were computed by setting a $5° \times 5°$ region around grid points concerned with a TC track for the month in which it occurred as missing values. This refinement showed no real impact on the greenhouse gas response pattern but rather slightly modulates it at some places (not shown). Since the two indices are expected to represent the potential for TC genesis, these should be compared with Fig. 8b. However, changes in TC genesis are broadly the same as for TC days, except that regions where changes are observed are generally located upstream of changes in TC days. Two exceptions can be noticed: the Eastern mid-latitudes and the North of the GoM. For the first region, it may reveal that although there should be

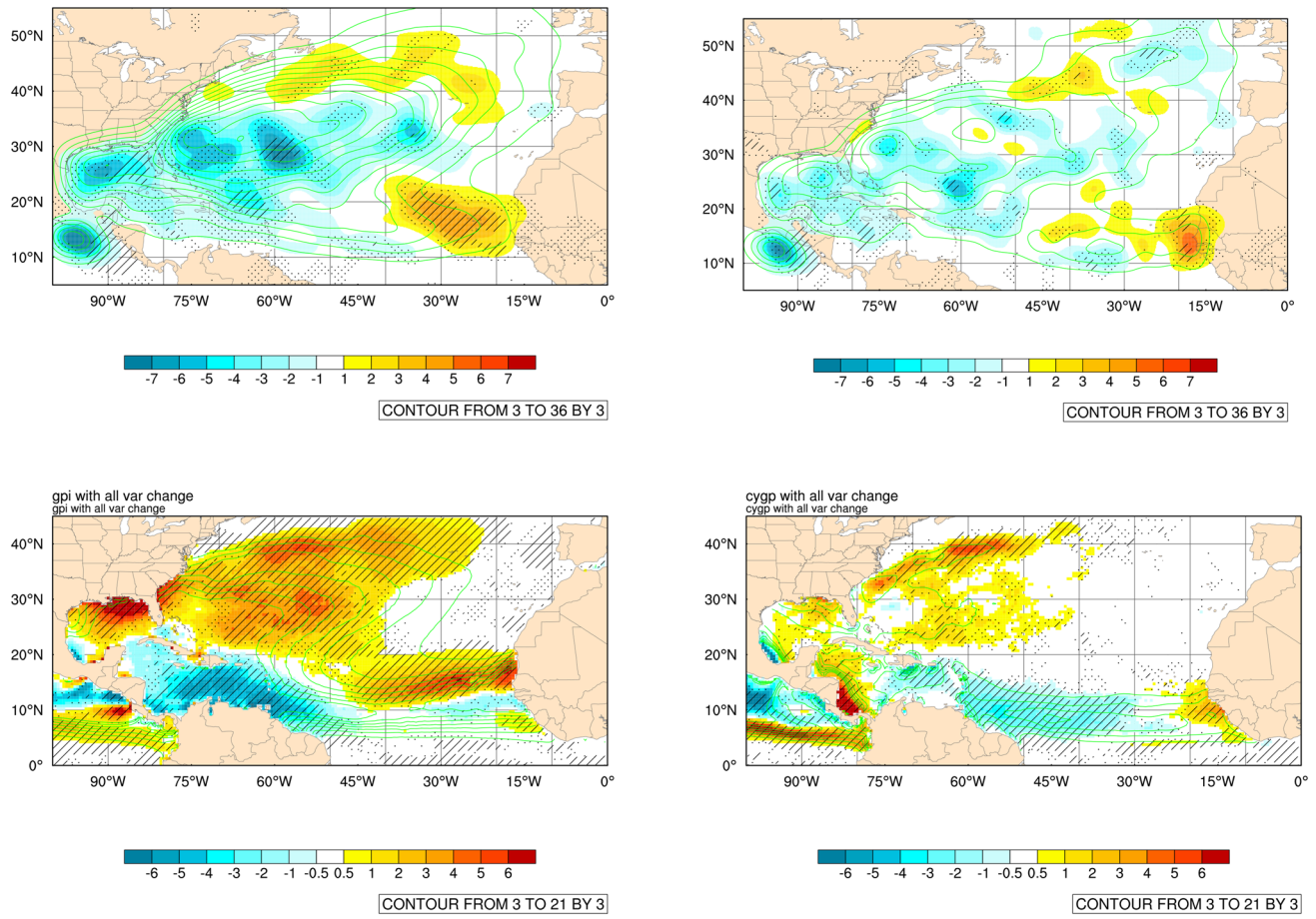

Fig. 8 Top: changes in the annual number of TC days (left) and TC genesis (right) densities between the future (AMIP-RCP85) and the present (AMIP-HIST) climate. Units are number of TC days per 20 years (left) or genesis per 50 years (right). Bottom: changes in the GPI (left) and CYGP (right) for the July–November season. Mean present climatology is reported as green contours. Dots and hatchings are for 95% and 99% significance levels respectively

less genesis in the future, systems may stay more time in their TC state, increasing the occurrence of TCs in the mid-latitudes. Given the similarities between TC days and TC genesis densities, cyclogenesis indices may still be valid for mature hurricanes (variables that forecasters look at during the hurricane season or in the seasonal reports are close to those contributing to cyclogenesis indices) (Klotzback et al. 2018 and references herein). Vertical wind shear is the most important of these predictors at the monthly to seasonal timescales, over the Eastern Pacific (Collins and Roache 2011) as well as Atlantic (Vecchi and Soden 2007). Thus, we will mostly consider TC days in the remainder of this paper since the studied sample size is larger and helps the statistical analysis. Figure 8c, d show the changes in the GPI and CYGP, respectively. While the overall changes between present and future climates are similar in the two indices, GPI and CYGP show large different patterns in some places.

Some broadscale similarities are evident between track, genesis densities and the cyclogenesis indices responses. The increase in the Eastern tropical Atlantic and mid-latitudes as well as the decrease in the western MDR are reproduced by the cyclogenesis indices. Nevertheless, some discrepancies appear at a more regional scale. In particular, the two indices do not capture the reduction in the subtropical Western Atlantic and GoM and show instead an increase. GPI shows a particularly large increase just North of the Tropic of Cancer that is opposite to both cyclogenesis and TC days. CYGP also have this bias but less marked than GPI. Moreover, the CYGP shows an increase in the western Caribbean Sea, opposite to the GPI signal and genesis density. This behavior is probably due to a bias in rainfall in this region where land proximity favors the triggering of convection. The subtropical discrepancy between genesis density and indices is more difficult to grasp. Some influencing components not taken into account in the indices probably play a role in the decrease of TC activity over this region. The reduction of the convective mass flux associated with the expansion of the tropics (Held and Zhao 2011) may be a good candidate

for the reduction in this region, which is not included in the cyclogenesis indices. Indeed, the only parameter that could take the reduction of the convective mass flux into account should be the convective precipitation used within the CYGP index. However, these regions are semi-desert and convective precipitation is very low.

The increase in TC activity in the Eastern tropical Atlantic is mainly captured by the CYGP index although slightly too South. GPI shows a tripolar pattern with a strong increase at the Mauritania latitude that does not correspond to the location of changes in TC days or genesis. This different behavior of the two indices is probably linked with the rainfall contribution to the CYGP. Given the position of the change pattern, one may expect that it is linked with some aspects of the African climate. A section will be dedicated to the link between this pattern and changes in AEWs.

4.1.3 Annual cycle of TC activity

Figure 9 shows the annual cycle of the number of tracks and track days for IBTrACS and the three ensemble simulations. Blue and green curves show that forcing the model by observed SSTs or bias-corrected model SSTs does not affect the annual cycle much. The model tends to underestimate the September peak of activity seen in IBTrACS and, to a lesser extent to overestimate the July activity. Moreover,

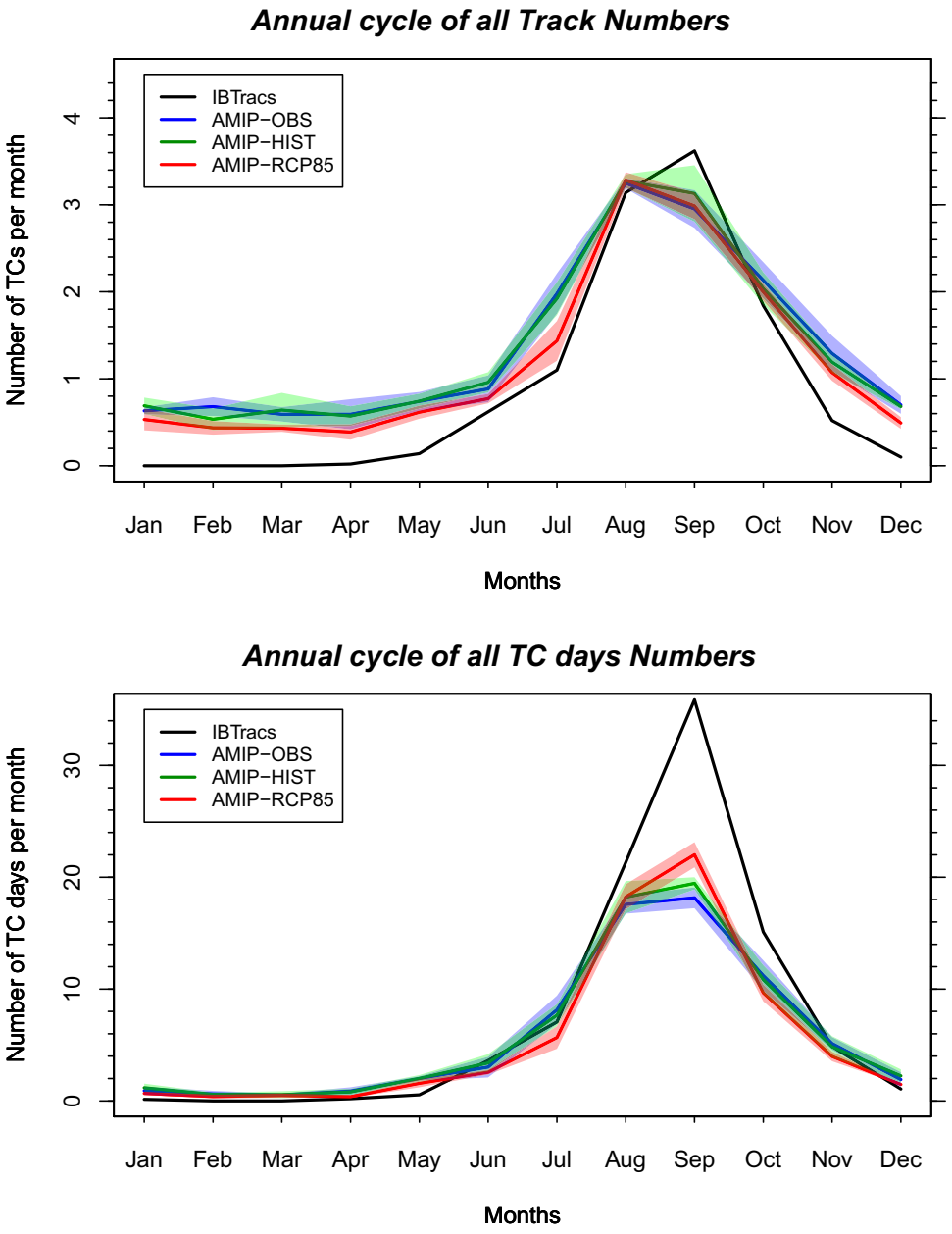

Fig. 9 Annual cycle of the number of tracks (top) and number of TC days (bottom) for IBTrACS (black) and the 3 ensemble runs, AMIP-OBS (blue), AMIP-HIST (green) and AMIP-RCP85 (red)

the model simulates residual TC activity all along the year that is mainly due to spurious tracks in some members of the ensemble (not shown). A noticeable point is that in the future climate the number of TCs is lower than in the present for nearly all months but only June, July and December are significant at the 95% level. The decrease is particularly noticeable in July for both TC number and TC days. This is coherent with Fig. 10 (top) showing the change in the number of TC days between present and future climates for the month of July. One can see a large reduction in TC days in the subtropical band without any counterbalance elsewhere in the basin. This may directly explain the seasonal changes

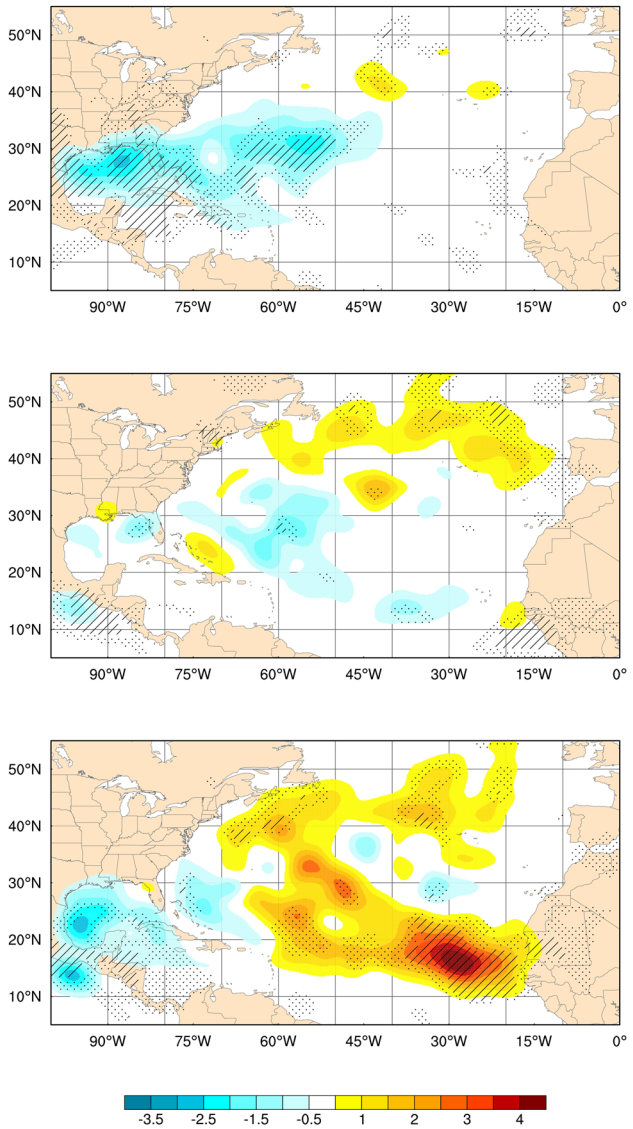

Fig. 10 Changes in the TC days between the future (AMIP-RCP85) and the present (AMIP-HIST) climate for months of July (top), August (middle) and September (bottom). Units are number of TC days per 20 years per 5°×5° square area. Dots (resp. hatching) are for 95% (resp. 99%) significance level

over this part of the Atlantic that was evident in Fig. 7a, b and that was not captured by the cyclogenesis indices. For the month of August there are no changes between the different sets of simulations although Fig. 10 (middle) shows a marked increase over the mid-latitudes compensated by a general decrease below 35° N. This corresponds to a broad northward shift in TC activity during August. September shows a quite different pattern of change compared with the two previous months. While numbers of TC tracks are not discernable between the present and future periods (Fig. 9a), TC days strongly increase (Fig. 9b). The large increase in TC days in the eastern tropical Atlantic is not compensated by the decrease in the GoM and East of Florida seen in Fig. 10. More generally, this figure shows that the main changes appearing on Fig. 8a, i.e. an increase in TC activity in the mid-latitudes and Cape-Verde region and a decrease in the tropical latitudes of the western Atlantic, occur at three different months and thus should be interpreted separately.

4.1.4 Annual cycle of TC genesis indices

As shown on Fig. 8, cyclogenesis indices have some difficulties to represent the different patterns of the number of TC days or TC genesis. The main drawback concerns subtropical latitudes around the GoM and Florida peninsula. In the following, we will address the components of the monthly TC genesis indices separately to understand the processes causing changes in TC days density, which are not captured by the indices. Figure 11 displays the components of these indices for the months of July, August and September. Since the CYGP and GPI share the vertical wind shear and vorticity components, we only show these two components as formulated in the GPI index (Emanuel and Nolan 2004). The other components are represented as they appear in GPI or CYGP (Royer et al. 1998). At first look, the different components show striking consistency in their monthly responses except for vorticity and, to some extent, relative humidity. Vorticity is the only component that shows a decrease over subtropical latitudes. Thus, the large decrease in TC days in July cannot be explained by the other variables. Given the monthly evolution of the changes in the vorticity component and their similarity with TC days decrease pattern, one may consider that the vorticity contribution is underestimated in the cyclogenesis indices. Potential intensity shows a strong increase over the mid-latitudes during the three months that can be related to a particularly warm SST anomaly (not shown) and is a good candidate to explain the mid-latitude poleward shift in TC days during August and September (Fig. 10). Elsewhere, however, it is opposite to TC densities. Vertical wind shear also shows a mid-latitude change favorable for genesis and TC occurrence. The change is maximum in July and August and may also account for the August maximum poleward shift. The humidity component of the

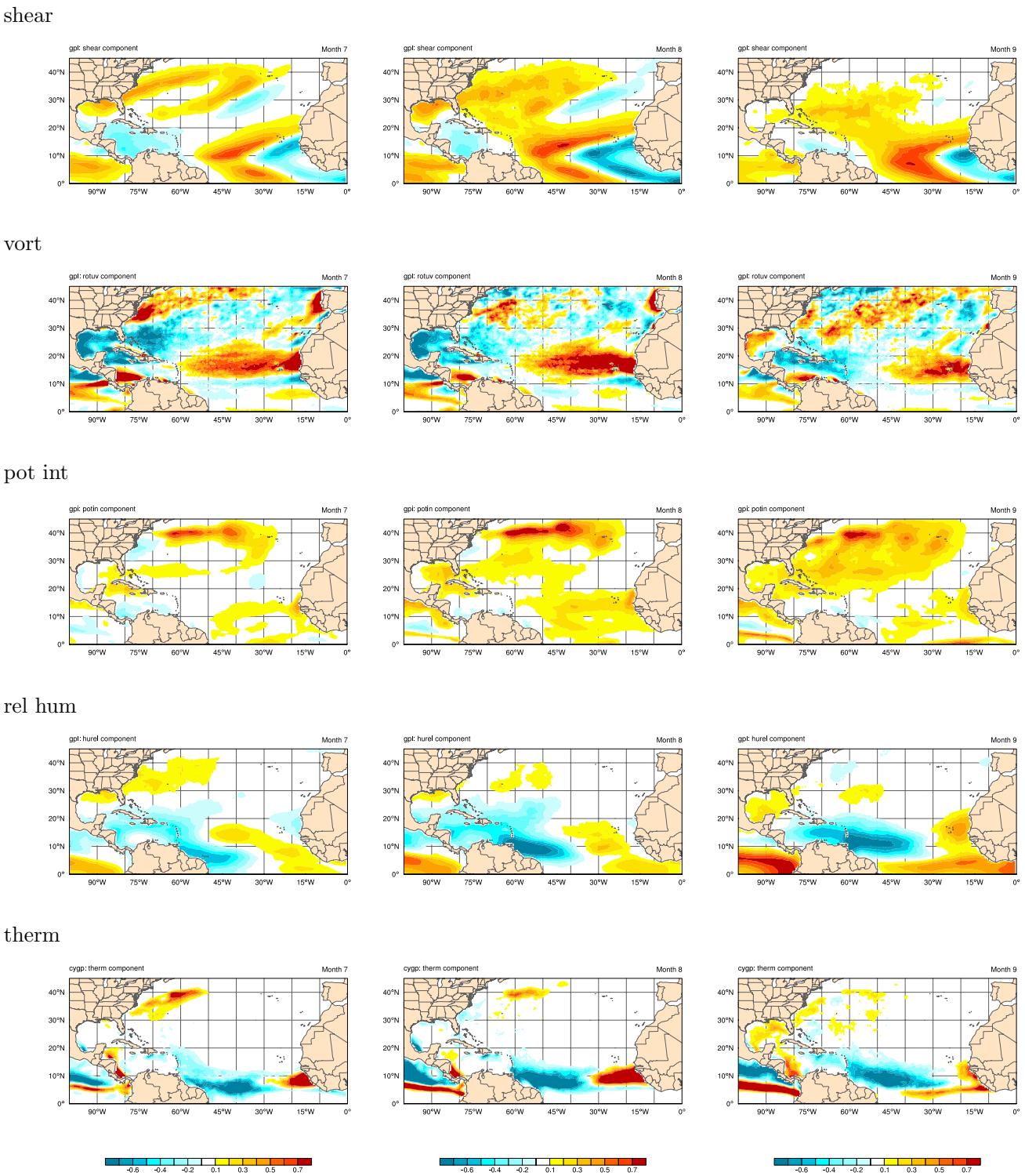

Fig. 11 Change in the individual components of the GPI and CYGP cyclogenesis, as they appear in the formula, for months of July (left), August (center) and September (right). Variables are listed by row as shear, vorticity, potential intensity, relative humidity components of the GPI and thermal component of the CYGP. The shear has been multiplied by 5 and the potential intensity by 2 to match the common legend box

GPI and thermal component of the CYGP also show a maximum response in July over these latitudes and thus may not be the key variables to explain the August maximum mid-latitude expansion. The MDR experiences different changes between its western and eastern parts (Fig. 8). As mentioned earlier, the eastern changes appear only in September and are well captured by the vorticity component as well as the two humidity-related components (relative humidity for the GPI and convective precipitation for the CYGP). Potential intensity suggests a decrease (resp. an increase) over the western (resp. eastern) MDR. The vertical shear component shows a complex change structure that could explain the western MDR decrease but not the eastern increase. Finally, the vorticity component may also partly explain the decrease in TC days in the western MDR. Thus, it is quite difficult to disentangle the respective roles of the different components over the Caribbean and GoM.

Overall, what can be said about cyclogenesis indices? At least that they are relevant to describe favorable environmental conditions thanks to a combination of their embedded components. Thus, the word "potential" used in the GPI acronym has been well chosen. Nevertheless they lack something that effectively drives actual TC activity in the model and that impacts the monthly behavior of this activity very differently. The weaknesses of the genesis indices may originate from the fact that relative contributions of favorable factors may vary during the season due in part to the spatial distribution of TC activity itself. Thus, ignoring such seasonal evolutions in the construction of the indices may explain their poor representativeness of the changing TC activity. Study of the individual components responses has not suggested such strong seasonal modulations, except the vorticity component which changes in July may explain subtropical latitude decrease in TC activity during this month. The strong increase in TC activity during September in the eastern part of the MDR may originate from the West African continent. This region has a dry-biased precipitation climatology in the historical runs and experiences a large increase in rainfall with climate warming (not shown). In the following, we perform some diagnostics relative to AEWs over the westernmost regions of Africa, which are susceptible to explain the processes at play in the large increase in TC days in future climate in September.

4.1.5 Relationship between TC activity and West African climate

It has been recognized for a long time that TC activity has some links with Sahelian rainfall (Landsea 1993), even though this relationship is most evident at the decadal time scale and may be due to simultaneous impacts of the AMO on both African climate and Atlantic TC activity. Nevertheless, since most major hurricanes that the Atlantic basin experiences originate from an AEW, African precursors can be investigated in an attempt to explain the September increase in TC days in the eastern tropical Atlantic (Fig. 10, bottom).

Figure 12 shows the change in the variance of the 2–6 days filtered meridional wind for July, August and September. This field can be seen as a raw measure of low level AEW activity (Albignat and Reed 1980; Mekonnen et al. 2006 among others). Indeed, Burpee (1972) showed that meridional wind presented a spectral peak at periods near 3–5 days between 850 and 600 hPa with a maximum at 700 hPa. Hsieh and Cook used a 725 hPa level to diagnose AEWs while Chauvin et al. (2005) used the 850 hPa vorticity. For an exhaustive study of AEWs, a finest definition of these would be necessary. Here, the purpose is to bring an explanation to the large TC activity change in September and a crude definition seems to be sufficient. A clear increase in AEW activity is noticeable over the westernmost part of the African continent as well as the adjacent ocean. There is indeed a change in the dynamics of AEWs peaking in August, which is coherent with the increase in the vorticity component of the cyclogenesis indices as well as the change in track density in September. However, it is not clear from Fig. 12 whether the increase in AEW activity is due to changes in meridional wind intensities or in the frequency of AEWs as well as why the AEW change is maximum in August while TC activity in the eastern Atlantic changes in September. Figure 13a, b show the distributions of the August and September AEW numbers for the present and future climates. Mean values are reported in Table 2. The number of AEWs have been defined as follows. To account for the occurrence of an AEW we computed a 6-hourly 850 hPa meridional wind average over a transect at 9° W (average between 8° W and 10° W) and a latitude band between 10° N and 20° N. For an AEW to be accounted for, 2–6 days filtered meridional wind is expected to be higher than a threshold. The latter is defined monthly as the mean over the 5 members of AMIP-Hist of the 2–6 days filtered meridional wind variance. Among all the consecutive steps that encompass the preceding condition, we select the maximum. Additionally, a change in direction of the filtered meridional wind (from North to South) must have occurred during a period of 4 days before the maximum across the region defined previously. A clear but small increase in the number of AEWs is evident for the future scenario, especially in August (Fig. 13a). This may partly explain the increase in TC activity during the peak TC season.

Figure 13c, d show the distributions of the time integrated absolute values of the meridional wind during the AEW crossing (i.e. over the 4 days preceding the maximum southerly wind which is located east of the AEW center). Changes in the intensity of AEWs is more evident in August than in September, in good agreement with changes in AEWs

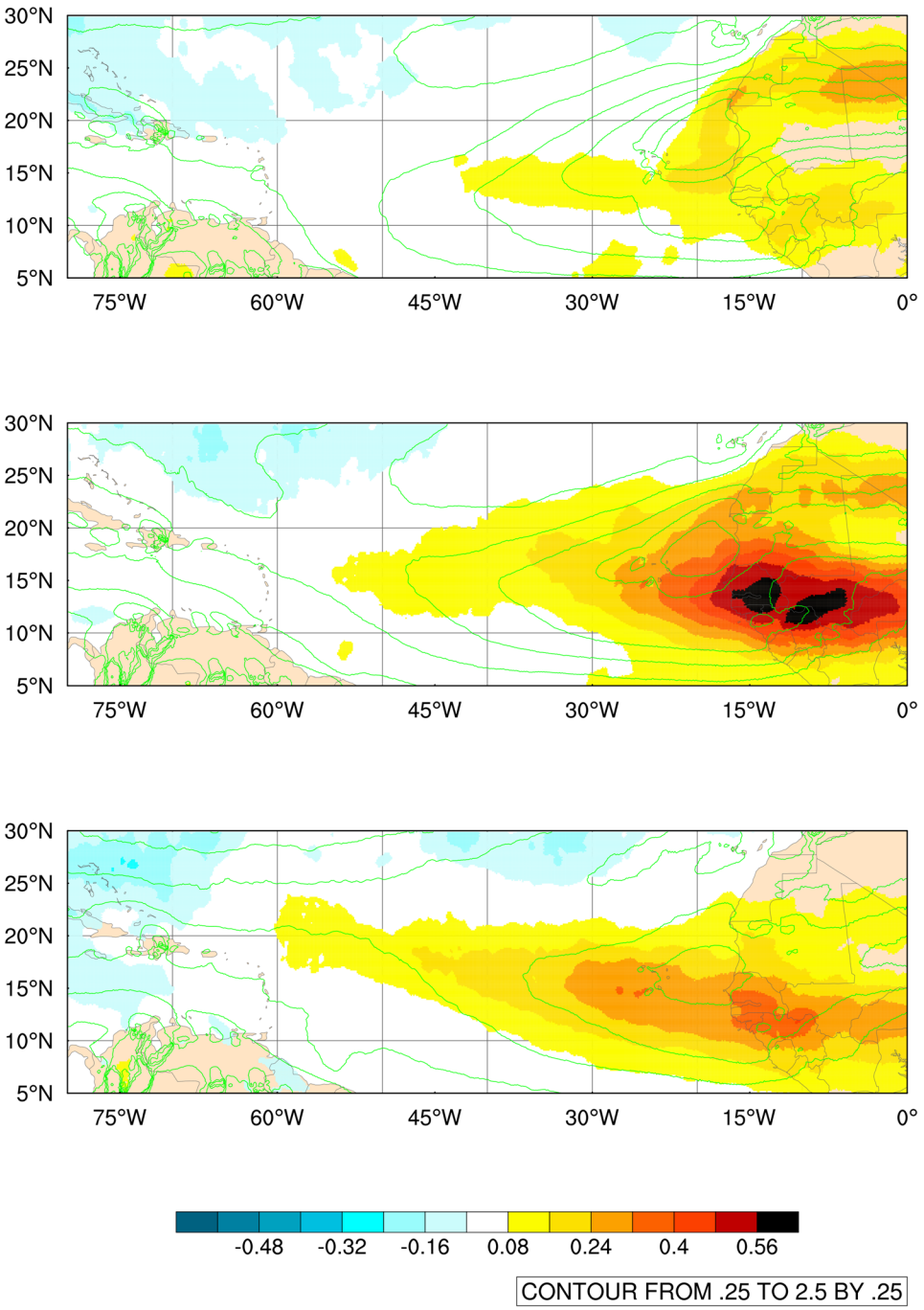

Fig. 12 Changes in the AEWs activity between the future (AMIP-RCP85) and the present (AMIP-HIST) climate for months of July (top), August (middle) and September (bottom). Units are ms^{-1}

activity in Fig. 12. Figure 13e, f show the distributions of accumulated AEW rainfall during August and September for the present and future climates. The distinction between the present and future distributions is more obvious than for the number of AEWs. Increase in AEW rainfall for August and September, as seen in Table 2, is around 15% which is coherent with the Clausius-Clapeyron formula with a warming of 2 K. Thus, it can be concluded that the increased TC activity in September may be explained partly by the increased number of AEWs crossing the Africa coast but above all by their moistening. The dynamics of AEWs seems to play a minor role in the increased eastern TC activity.

The question that arises now is why TC activity is largely increased in September instead of August which experiences a quite stronger change in AEW activity. No clear signal could be found into cyclogenesis components changes to highlight this particularity. In fact, when addressing the vertical shear of the horizontal wind, we only considered the 850 and 200 hPa levels, with the underlying hypothesis that nothing occurred between these two levels. However, Africa

is an exception for the Atlantic basin. Indeed, the summer monsoon as well as AEWs that develop during this season are largely modulated by the mid-level African easterly jet which takes place between 10° and 20° N. AEWs draw their energy from this jet which covers the western Africa as well as the eastern Atlantic (Hsieh and Cook 2005). A resulting shear in the wind between the Jet and lower or upper levels can induce unfavorable conditions for TC development (Dunion and Velden 2004). Figure 14 shows the shear between 850 and 600 hPa for July, August and September as a function of latitude for present and future climate. One can notice than during July and August, the shear is marked and increases in the future climate. At the contrary, September shows a low shear with a small increase in the future. Thus, increase in the September TC activity may be explained by a combination of increased AEW activity in a low shear environment. By opposition August is marked by a stronger AEW activity increase but in a high shear environment. This result emphasizes the role of AEW activity in the following TC activity, although Patricola et al. (2017) found that the link between the two processes was not obvious at the seasonal timescale. Indeed, by simulating the active 2005 cyclonic season with a regional model for which AEWs were suppressed or not as lateral boundary condition, they found that the seasonal activity was not really changed at the scale of the whole Atlantic basin. Here, the 50-year ensemble simulations suggest that the relationship between AEWs and TC activity may be strong in the eastern Atlantic in a climate change perspective. It suggests that African climate as well as its changes with a warming climate may be important to address the changes in TC activity. This result is not in contradiction with Patricola et al. (2017) since, contrarily to them, we consider only the eastern part of the Atlantic basin but for two 50-year 5-member ensemble simulations.

The link that we emphasized in this study may, however, be highly model-dependent since changes in African climate is far from having reached a consensus among models in the previous CMIP exercises (Stocker et al. 2013). Moreover, African climate may become another source of uncertainty when all the effects of mineral dusts will be taken into account in the GCMs. The evolution of the Saharan Air Layer (Dunion and Velden 2004) will provide another source of uncertainty for the evolution of Atlantic TCs.

4.2 Changes in TC composites

4.2.1 Composite wind speed

One major threat associated with TCs is obviously the wind speed and changes in this field are important to investigate. As shown on Table 1, mean changes in maximum wind speed and minimum sea level pressure are small while statistically significant. Here we constructed TC-centered composite fields to assess the horizontal structures of these changes. Since wind intensities are quite realistic in the simulations due to the high resolution of the model, we distinguished tropical storms (TS), hurricanes (Hu) and major hurricanes (MH). This distinction follows the Saffir–Simpson scale (Simpson and Saffir 1974). Figure 15 shows the composite wind speed changes for TS (top), Hu (middle) and MH (bottom) between the present and future climates for both West Indies (left) and eastern MDR (right). Since the structure of the TC field may have changed after their recurving at tropical or extra-tropical latitudes, we also distinguished between TCs over mid-latitudes and over the tropics. Results for mid-latitudes are shown on Fig. S1 for completeness but are not commented. The tropics were separated between the Eastern Main Development Region (EMDR) and an extended West Indies region. The EMDR has been defined in order to cover the region 5°–20° N and 40°–0° W and the West Indies region covers the Caribbean and Western MDR (10°–20° N and 80°–40° W). The distinction between these two regions was suggested by the different changes shown on Fig. 8.

While changes over the West Indies are detectable only for MH in the Northeastern quadrant and are relatively small, changes over the EMDR are more marked, especially for MH, which show increases reaching 5 ms^{-1} that account for approximately 10% of wind intensity. This confirms the marked increase in TC activity over the Cape Verde region described earlier. These results are in good agreement with the main results from IPCC AR5 indicating that the strongest TCs may become stronger (Stocker et al. 2013). Chauvin et al. (2006) already suggested this tendency with a previous version of the ARPEGE-Climat model but the lower resolution and the shorter simulation length did not allow to separate different classes of TCs.

4.2.2 Composite rainfall

Figure 16 shows rainfall changes inside TCs Over West Indies (left) and eastern MDR (right). Changes for mid-latitudes are reported on Fig. S2. As in previous studies (Chauvin et al. 2006, 2017; Knutson et al. 2013), the change in rainfall is comprised between 5 and 15% according to the distance from the center of the TC. Statistically significant patterns appear for each TC class although not always located over the peak in rainfall change. Since we decomposed the signal between three classes, sampling constraints are stronger than if all categories were considered together. However, this result seems to be quite robust given that the version of the model we have used in this study has radically different parameterization schemes than the one used by Chauvin et al. (2006, 2017). In the latter reference, a systematic study of TC rainfall was undertaken and it was shown that the TC rainfall increase with global warming broadly

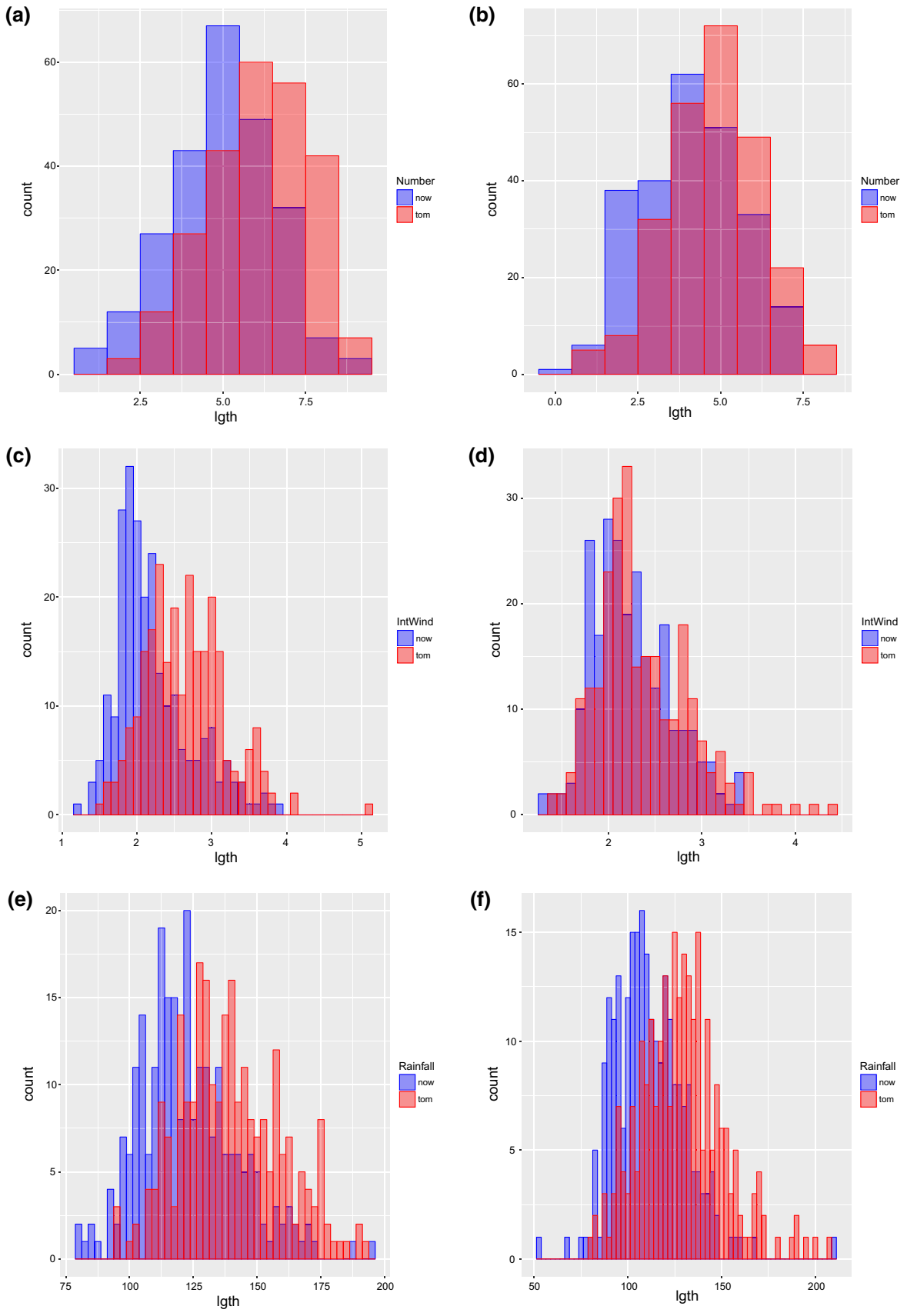
(a)
count
lgth
Number
now
tom
(b)
count
lgth
Number
now
tom
(c)
count
lgth
IntWind
now
tom
(d)
count
lgth
IntWind
now
tom
(e)
count
lgth
Rainfall
now
tom
(f)
count
lgth
Rainfall
now
tom

◂**Fig. 13** Histograms of yearly number (top), time integrated meridional wind intensity (ms^{-1}; middle) and accumulated rainfall (mm day^{-1}; bottom) for AEWs crossing the 9° W longitude between 5° and 20° N. Left (resp. right) panels **a**, **c** and **e** (resp. **b**, **d** and **f**) are for the month of August (resp. September)

follows the Clausius–Clapeyron formula except for extreme rainfall that may increase at twice this rate. An interesting result to mention is the increase over the West Indies region. Indeed, the rainfall increase for Hu and MH shows a clear eastward spread of the rainfall maximum, suggesting that a broader region within TCs will experience intense rainfall.

5 Conclusion

As a conclusion, one can understand that cyclogenesis indices still have some issues to address the response of TC activity to climate change. Many reasons can be highlighted but it seems to us that their main shortcomings can be summarized as follows. The variables used to construct the cyclogenesis indices are accurate to account for the probability of cyclogenesis at the daily timescale. By extrapolation, the combination of their monthly values has shown a relatively good ability to represent the climatology of TC genesis (Gray 1975; Royer et al. 1998; McDonald et al. 2005; Camargo et al. 2007). Nevertheless, as soon as variability has to be addressed, some difficulties arise, from the interannual (Menkes et al. 2012) to the climate change scale (Royer and Chauvin 2009). To our knowledge, the only success for cyclogenesis indices is for the ENSO variability that has been proven to be well captured by these indices (Menkes et al. 2012; Camargo et al. 2007). The explanation is probably that ENSO is a strong and long-lasting mode of variability, whose signature in the atmosphere is coherent for several months. Thus, monthly anomalies of variables favorable for genesis will also be coherent all along the hurricane season. In other cases, long-term anomalies are weaker and their effects may be more or less marked and not necessarily well captured by the monthly averages. If one could construct cyclogenesis indices at the weekly or daily timescale and integrate them over time, there might be better agreement between the indices and actual TC activity. Yet doing so is far from being easy since one should eliminate the effect of the TCs themselves on the environment. Although it was shown that the impact of TC removal was modest at the monthly timescale, the TC response at a shorter timescale may locally impact the long-term behavior of the indices. In this study, we showed that the long-term response can also vary from one month to another, meaning that there is probably an interaction between the TC response and the annual cycle of TC activity that cyclogenesis indices have some difficulties to integrate.

Finally, notwithstanding that cyclogenesis indices are expected to represent some potential for genesis, real birth of TC systems follows some stochastic rules (Jourdain et al. 2011), which may contradict the response between indices and real TCs.

In conclusion, with the increasing resolution of climate models, the issue of cyclogenesis indices will probably be solved with direct TC counts. However, direct detection of TCs is far from being the final method to assess the climate change response. Indeed, TCs are thermal machines, which depend on several subgrid-scale processes that must be parameterized and thus may induce some biases in TC activity. The large-scale approach may in this case be complementary with the direct approach. Here, in this study, showing how TC genesis may change in a future climate over the MDR is poorly possible with the direct approach since TC climatology is biased toward the mid-latitudes. Cyclogenesis indices still seem to provide useful information. Even though the progress in computing allows to enhance the

Table 2 Mean statistics of AEW characteristics for the months of August and September

	August	September
Number	5/6.1**	4.1/4.8 **
Merid. wind absolute value (ms^{-1})	2.2/2.6**	2.2/2.4*
Rainfall (mm day^{-1})	123/139**	111/129**

First number is for AMIP-Obs and the second for AMIP-RCP85. * (resp. **) indicates that the change is significant at the 99% (resp. 99.9%) level

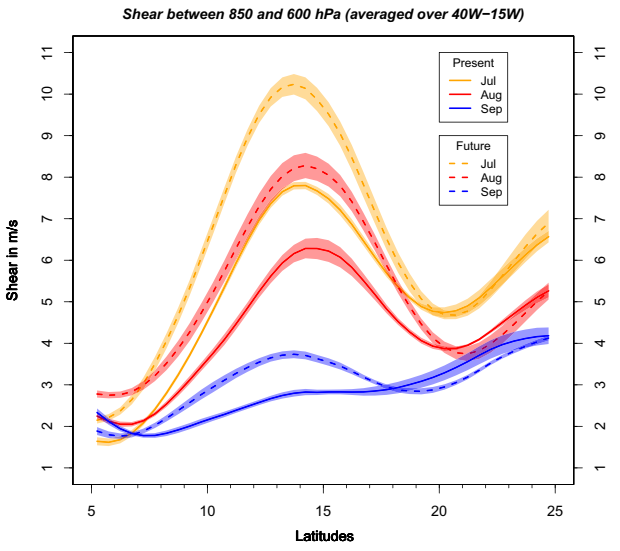

Fig. 14 Averaged shear of the horizontal wind between 850 and 600 hPa over the eastern MDR. The average have been done over the domain 5°–25° N and 40°–15° W. Units are ms^{-1}

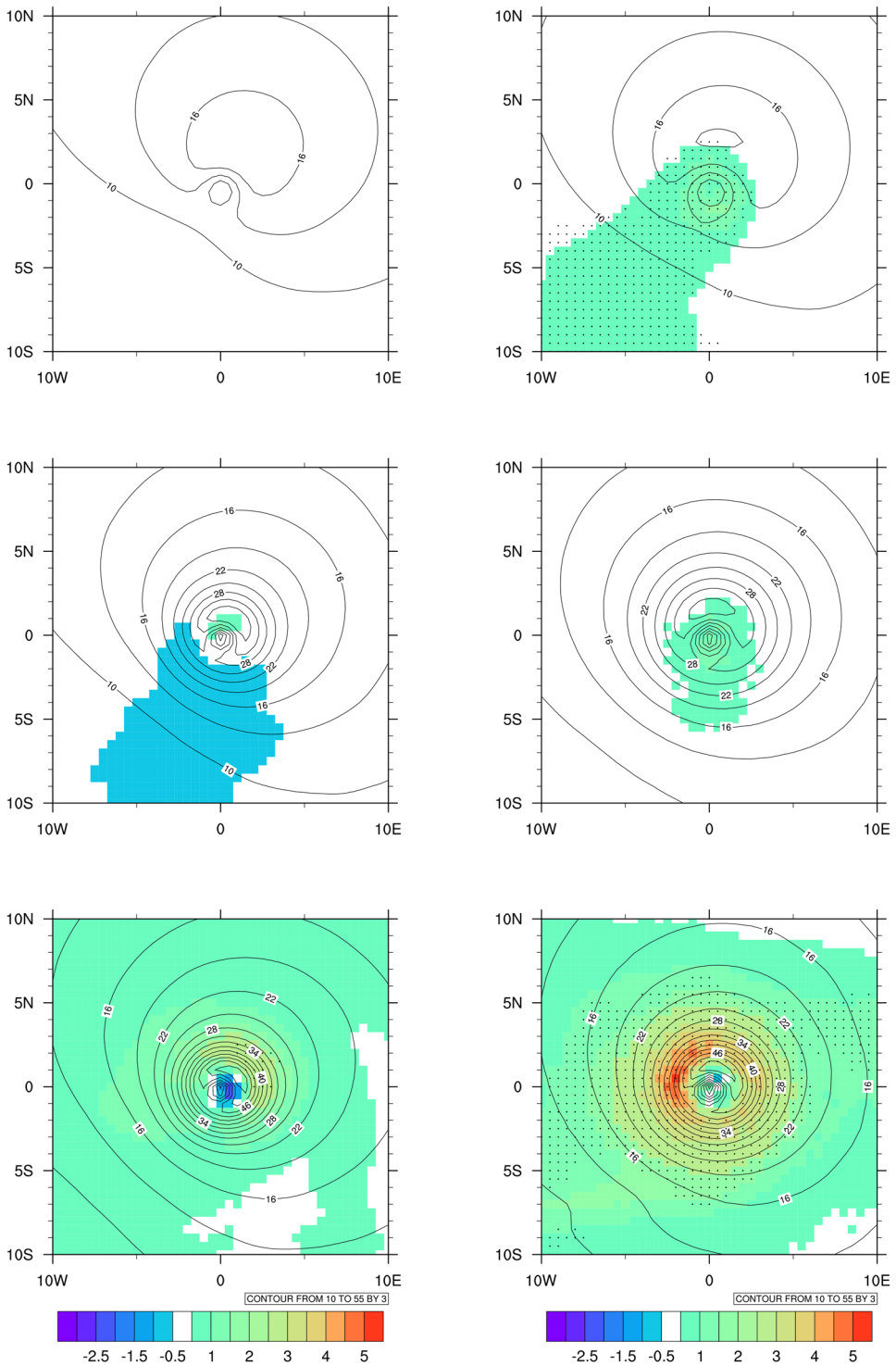

Fig. 15 Composite change of wind speed (ms^{-1}) for West Indies (left) and EMDR (right) for the tropical storms (top), hurricanes (middle) and major hurricanes (bottom) between future and present simulations. Contours are the present mean value and dots are for 95% significance level

spatial resolution of climate models and direct detection of strong TCs, the prohibitive cost of such simulations is still a limiting factor for massive ensemble high-resolution model intercomparison. Besides, part of the increasing computing resources has to be used for ocean–atmosphere coupling that was not considered in this study but is an important feature to take into account to provide a full overview of the sensitivity of TC activity to climate change. Preliminary work by Daloz et al. (2012) addressed the effects of rotation-stretching in a coupled simulation and showed that the configuration

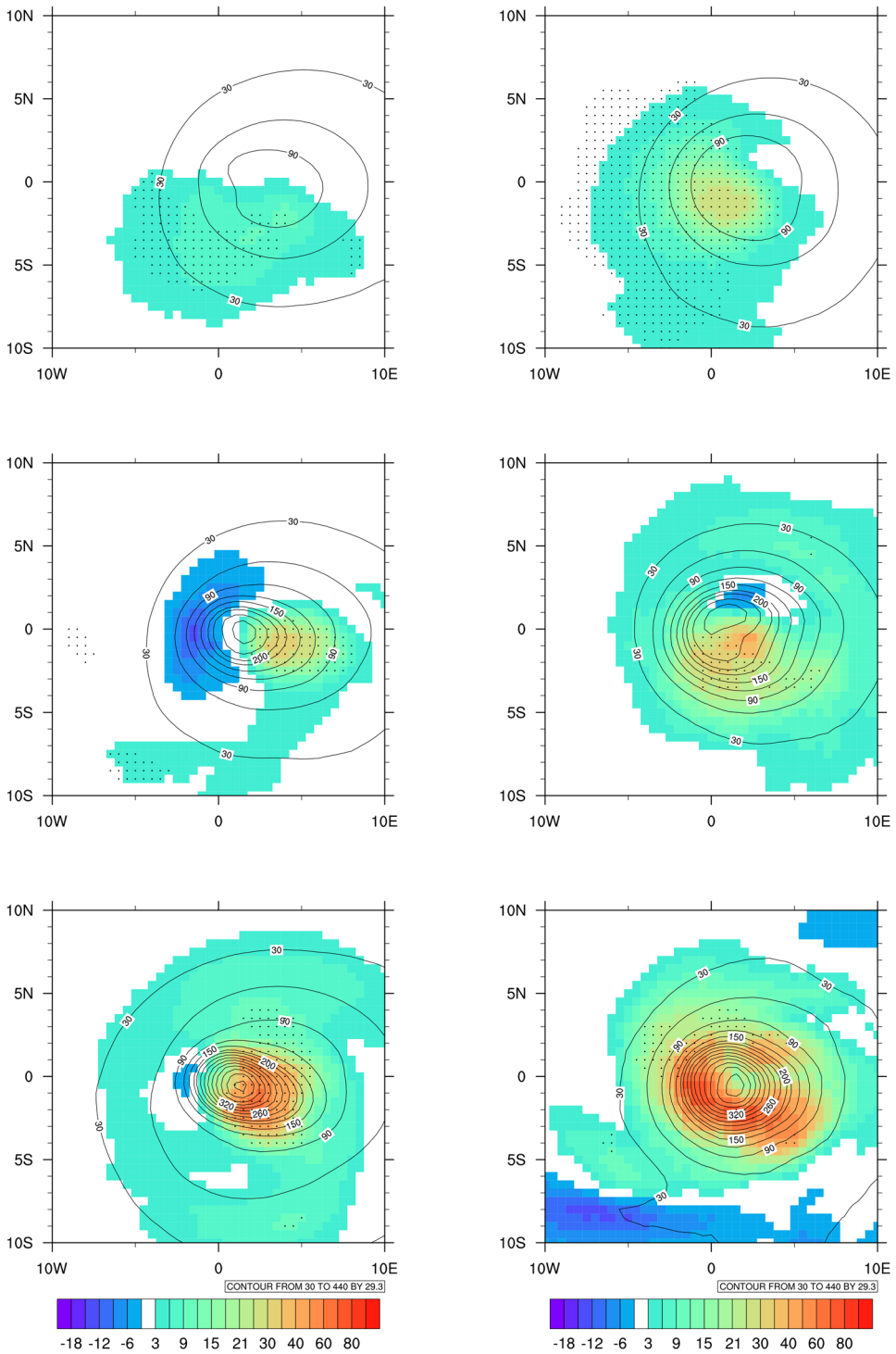

Fig. 16 Same as Fig. 15 for rainfall (mm day^{-1})

was accurate for climate change studies even though we may expect weakest TCs due to the feedback of TC cold wake on its lifetime. Cyclogenesis indices may still be appropriate for climate change studies for several years yet, particularly if some similarities between responses of indices and objectively detected TCs may be highlighted. This is one of the questions that should be addressed in coming studies to allow taking into account the full potential of CMIP databases.

Acknowledgements This study has been funded by the ERDF project C3AF (Changement Climatique et Conséquences sur les Antilles Françaises, Grant number CR/16-115).

Appendix: Computation of the density of TC genesis and TC days

A simple way to calculate the density of genesis or occurrence of a TC is to increment the value at the gridpoint underlying the genesis or TC track position by 1 for all the tracks over a given period. Thus by dividing the counts by the surface of the gridpoint, a density is obtained. Nevertheless, this method depends on the grid over which counting is performed. For very fine grids the results can show very local structures that may be difficult to interpret. Indeed, some gridpoints will never see any track while neighbours will do so. Spatial filtering can thus be used to homogenize the results. One can decide to average the number of TC occurrences over a defined area. In this study, the counting has been performed according to the following method.

For each gridpoint, TC occurrences over the neighbouring gridpoints are accounted for according to their distance to the gridpoint. A gaussian weighting is calculated according to a reference radius of 200 km. For a TC located at the radius distance from the gridpoint, the weight is $(1/e)^{0.5}$, according to the exponential formulation of the gaussian weight ($w = e^{-0.5*(dist/radius)^2}$) with *dist* being the distance of the gridpoint to the track occurrence. The resulting density presents the advantage of being a continuous field independent of the projection grid. Smoothness of the density can be calibrated by the choice of the reference radius. The radius was chosen so that the influence of a TC occurrence is realistic. It was assumed that a radius of 200 km was a good choice since the weight at higher distances is not zero but decreases exponentially. One consequence of the density calculation is that the total number of TC genesis or occurrences over the basin should be expected by the spatial average rather than sum of the density field.

References

Albignat J-P, Reed RJ (1980) The origin of African wave disturbances during phase III of GATE. Mon Weather Rev 108:1827–1839

Atkinson GD, Holliday CR (1977) Tropical cyclone minimum sea level pressure/maximum sustained wind relationship for the western North Pacific. Mon Weather Rev. https://doi.org/10.1175/1520-0493

Bell GD, Chelliah M (2006) Leading tropical modes associated with interannual and multidecadal fluctuations in North Atlantic hurricane activity. J Clim 19:590–612

Bengtsson L, Hodges KI, Esch M, Keenlyside N, Kornblueh L, Luo J-J, Yamagata T (2007) How may tropical cyclones change in a warmer climate? Tellus A 59:539–561

Beven JL, Avila LAL, Blake ES, Brown DP, Franklin JL, Knabb RD, Pasch RJ, Rhome JR, Stewart SR (2007) Atlantic hurricane season of 2005. Mon Weather Rev 136:1109–1173

Bhatia K, Vecchi G, Murakami H, Underwood S, Kossin J (2018) Projected response of tropical cyclone intensity and intensification in a global climate model. J Clim 31:8281–8303

Bister M, Emanuel KA (1998) Dissipative heating and hurricane intensity. Meteorol Atmos Phys. https://doi.org/10.1007/bf01030791

Burpee RW (1972) The origin and structure of easterly waves in the lower troposphere of North Africa. J Atmos Sci 29:70–90

Camargo SJ, Emanuel KA, Sobel AH (2007) Use of a genesis potential index to diagnose ENSO effects on tropical cyclone genesis. J Clim 20:4819–4834. https://doi.org/10.1175/JCLI4282.1

Chauvin F, Royer J-F, Douville H (2005) Interannual variability and predictability in a GCM. Clim Dyn 24:523–544

Chauvin F, Royer J-F, Déqué M (2006) Response of hurricane-type vortices to global warming as simulated by ARPEGE-Climat at high resolution. Clim Dyn 27:377–399. https://doi.org/10.1007/s00382-006-0135-7

Chauvin F, Douville H, Ribes A (2017) Atlantic tropical cyclones water budget in observations and CNRM-CM5 model. Clim Dyn. https://doi.org/10.1007/s00382-017-3559-3

Collins JM, Roache DR (2011) The 2009 hurricane season in the eastern North Pacific basin: an analysis of environmental conditions. Mon Weather Rev 139:1673–1682. https://doi.org/10.1175/2010MWR3538.1

Courtier P, Geleyn J-F (1988) A global numerical weather prediction model with variable resolution: application to the shallow-water equations. Q J R Meteorol Soc 114(483):1321–1346. https://doi.org/10.1002/qj.49711448309

Cuxart J, Bougeault P, Redelsperger JL (2000) A turbulence scheme allowing for mesoscale and large-eddy simulations. Q J Roy Meteor Soc 126:1–30. https://doi.org/10.1002/qj.49712656202

Daloz A-S, Chauvin F, Roux F (2012) Impact of the configuration of stretching and ocean-atmosphere coupling on tropical cyclone activity in the variable-resolution {GCM ARPEGE}. Clim Dyn 39:2343–2359. https://doi.org/10.1007/s00382-012-1561-3

Déqué M, Piedelievre J-P (1995) High-Resolution climate simulation over Europe. Clim Dyn 11:321–339

Done JM, Bruyère CL, Ge M, Jaye A (2014) Internal variability of North Atlantic tropical cyclones. J Geophys Res Atmos 119:6506–6519. https://doi.org/10.1002/2014JD021542

Dunion JP, Velden CS (2004) The impact of the Saharan air layer on Atlantic tropical cyclone activity. Bull Am Meteorol Soc. https://doi.org/10.1175/bams-85-3-353

Emanuel KA (2013) Downscaling CMIP5 climate models shows increased tropical cyclone activity over the 21st century. Proc Natl Acad Sci USA 110:12219–12224. https://doi.org/10.1073/pnas.1301293110

Emanuel KA (2015) Effect of upper-ocean evolution on projected trends in tropical cyclone activity. J Clim 28:8165–8170. https://doi.org/10.1175/JCLI-D-15-0401.1

Emanuel KA, Nolan DS (2004) Tropical cyclone activity and the global climate system. In: 26th conference on hurricanes and tropical meteorology. American Meteorological Society, Miami, FL

Fox-Rabinovitz M, Côté J, Dugas B, Déqué M, McGregor JL (2006) Variable resolution general circulation models: stretched-grid model intercomparison Niño project (SGMIP). J Geophys Res 111:D16104. https://doi.org/10.1029/2005JD006520

Gibelin A-L, Déqué M (2003) Anthropocentric climate change over the Mediterranean region simulated by a global variable resolution model. Clim Dyn 20:327–339

Goldenberg SB, Shapiro LJ (1996) Physical mechanisms for the association of El Niño and west African rainfall with Atlantic major hurricane activity. J Clim. https://doi.org/10.1175/1520-0442(1996)009%3c1169:PMFTAO%3e2.0.CO;2

Goldenberg SB, Landsea CW, Mestas-Nuñez AM, Gray WM (2001) The recent increase in Atlantic hurricane activity: Causes and implications. Science (80-) 293:474–479. https://doi.org/10.1126/science.1060040

Gray WM (1968) Global view of the origin of tropical disturbances and storms. Mon Weather Rev. https://doi.org/10.1175/1520-0493(1968)096%3c0669:GVOTOO%3e2.0.CO;2

Gray WM (1975) Tropical cyclone genesis. Department of Atmospheric Science Colorado State University, Fort Collins, p 121

Gueremy JF (2011) A continuous buoyancy based convection scheme: one- and three-dimensional validation. Tellus Ser A Dyn Meteorol Oceanogr. https://doi.org/10.1111/j.1600-0870.2011.00521.x

Haarsma RJ et al (2016) High resolution model intercomparison project (HighResMIP v1.0) for CMIP6. Geosci Model Dev. https://doi.org/10.5194/gmd-9-4185-2016

Harris LM, Lin S-J, Tu CY (2016) High-resolution climate simulations using GFDL HiRAM with a stretched global grid. J Clim 29:4293–4313. https://doi.org/10.1175/jcli-d-15-0389.1

Held IM, Zhao M (2011) The response of tropical cyclone statistics to an increase in CO_2 with fixed sea surface temperatures. J Clim. https://doi.org/10.1175/JCLI-D-11-00050.1

Hsieh J-S, Cook KH (2005) Generation of African easterly waves disturbances: relationship to the African easterly jet. Mon Weather Rev 133:1311–1327

Jourdain NC, Marchesiello P, Menkes CE, Lefèvre J, Vincent EM, Lengaigne M, Chauvin F (2011) Mesoscale simulation of tropical cyclones in the south pacific: climatology and interannual variability. J Clim. https://doi.org/10.1175/2010JCLI3559.1

Klotzback PJ, Schreck CJ III, Collins JM, Bell MM, Blake ES, Roache DR (2018) The extremely active 2017 North Atlantic hurricane season. Mon Weather Rev 146:3425–3443. https://doi.org/10.1175/MWR-D-18-0078.1

Knapp KR, Kruk MC, Levinson DH, Diamond HJ, Neumann CJ (2010) The international best track archive for climate stewardship (IBTrACS) unifying tropical cyclone data. Bull Am Meteorol Soc 91:363–376

Knutson TR et al (2010) Tropical cyclones and climate change. Nat Geosci 3:157–163. https://doi.org/10.1038/ngeo779

Knutson TR et al (2013) Dynamical downscaling projections of twenty-first-century Atlantic hurricane activity: CMIP3 and CMIP5 model-based scenarios. J Clim 26:6591–6617

Knutson TR, Sirutis JJ, Zhao M (2015) Global projections of intense tropical cyclone activity for the late twenty-first century from dynamical downscaling of CMIP5/RCP4.5 scenarios. J Clim 28:7203–7224. https://doi.org/10.1175/JCLI-D-15-0129.1

Kossin JP, Emanuel KA, Vecchi GA (2014) The poleward migration of the location of tropical cyclone maximum intensity. Nature 509:349–352

Landsea CW (1993) A climatology of intense (or major) Atlantic hurricanes. Mon Weather Rev. https://doi.org/10.1175/1520-0493(1993)121%3c1703:ACOIMA%3e2.0.CO;2

Li H, Sriver RL (2018) Tropical cyclone activity in the high-resolution community earth system model and the impact of ocean coupling. J Adv Model Earth Syst 10:165–186. https://doi.org/10.1002/2017MS001199

Li H, Sheffield J, Wood EF (2010) Bias correction of monthly precipitation and temperature fields from Intergovernmental Panel on Climate Change AR4 models using equidistant quantile matching. J Geophys Res Atmos. https://doi.org/10.1029/2009JD012882

Lopez P (2002) Implementation and validation of a new prognostic large-scale cloud and precipitation scheme for climate and data-assimilation purposes. Q J Roy Meteor Soc 128:229–257. https://doi.org/10.1256/00359000260498879

Lorant V, Royer JF (2001) Sensitivity of equatorial convection to horizontal resolution in aqua-planet simulations with variable-resolution GCM. Mon Weather Rev 129:2730–2745

Masson V et al (2013) The SURFEXv7.2 land and ocean surface platform for coupled or offline simulation of earth surface variables and fluxes. Geosci Model Dev. https://doi.org/10.5194/gmd-6-929-2013

McDonald R, Bleaken D, Cresswell D, Pope V, Senior C (2005) Tropical storms: representation and diagnosis in climate models and the impacts of climate change. Clim Dyn. https://doi.org/10.1007/s00382-004-0491-0

Mekonnen A, Thorncroft CD, Aiyyer AR (2006) Analysis of convection and its association with African easterly waves. J Clim 19:5405–5421

Menkes CE, Lengaigne M, Marchesiello P, Jourdain NC, Vincent EM, Lefèvre J, Chauvin F, Royer JF (2012) Comparison of tropical cyclogenesis indices on seasonal to interannual timescales. Clim Dyn. https://doi.org/10.1007/s00382-011-1126-x

Murakami H, Wang B (2010) Future change of North Atlantic tropical cyclone tracks: projection by a 20-km-mesh global atmospheric model. J Clim 23:2699–2721. https://doi.org/10.1175/2010JCLI3338.1

Murakami H, Mizuta R, Shindo E (2012a) Future changes in tropical cyclone activity projected by multi-physics and multi-SST ensemble experiments using the 60-km-mesh MRI-AGCM. Clim Dyn 39:2569–2584. https://doi.org/10.1007/s00382-011-1223-x

Murakami H et al (2012b) Future changes in tropical cyclone activity projected by the new high-resolution MRI-AGCM. J Clim 25:3237–3260. https://doi.org/10.1175/JCLI-D-11-00415.1

Oouchi K, Yoshimura J, Yoshimura H, Mizuta R, Kusunoki S, Noda A (2006) Tropical cyclone climatology in a global-warming climate as simulated in a 20 km-mesh global atmospheric model: frequency and wind intensity analyses. J Meteorol Soc Jpn Ser II. https://doi.org/10.2151/jmsj.84.259

Ooyama K (1969) Numerical simulation of the life cycle of tropical cyclones. J Atmos Sci. https://doi.org/10.1175/1520-0469(1969)026%3c0003:NSOTLC%3e2.0.CO;2

Ooyama KV (1982) Conceptual evolution of the theory and modeling of the tropical cyclone. J Meteorol Soc Jpn Ser II. https://doi.org/10.2151/jmsj1965.60.1_369

Pasch RJ, Blake ES, Cobb III HD, Roberts DP (2006) Tropical cyclone report, Hurricane Wilma, 15–25 October 2005. National Hurricane Center

Patricola CM, Saravanan R, Chang P (2017) The response of Atlantic tropical cyclones to suppression of African easterly waves. Geophys Res Lett 45:471–479. https://doi.org/10.1002/2017GL076081

Piriou J-M, Redelsperger J-L, Geleyn J-F, Lafore JP, Guichard F (2007) An approach for convective parameterization with memory: Separating microphysics and transport in grid-scale equations. J Atmos Sci 64(11):4127–4139. https://doi.org/10.1175/2007jas2144.1

Powell MD, Houston SH, Reinhold TA (1996) Hurricane Andrew's landfall in South Florida, Part I: standardizing measurements for documentation of surface wind fields. Weather Forecast 11:329–349

Royer JF, Chauvin F (2009) Response of tropical cyclogenesis to global warming in an IPCC AR4 scenario. In: Elsner J, Jagger T (eds) Hurricanes and climate change. Springer, Boston, MA

Royer JF, Chauvin F, Timbal B, Araspin P, Grimal D (1998) A GCM study of the impact of greenhouse gas increase on the frequency of occurrence of tropical cyclones. Clim Change. https://doi.org/10.1023/a:1005386312622

Simpson RH, Saffir H (1974) The hurricane disaster-potential scale. Weatherwise 27(4):169

Staten PW, Lu J, Grise KM, Davis SM, Birner T (2018) Re-examining tropical expansion. Nat Clim Change 8:768–775. https://doi.org/10.1038/s41558-018-0246-2

Stocker TF, Qin D, Plattner GK, Tignor M, Allen SK, Boschung J, Nauels A, Xia Y, Bex V, Midgley PM (eds) (2013) IPCC, 2013: Climate change 2013: the physical science basis. Contribution of working group I to the fifth assessment report of the intergovernmental panel on climate change. Cambridge University Press, Cambridge, UK, New York, NY, USA

Sugi M, Murakami H, Yoshimura J (2009) A reduction in global tropical cyclone frequency due to global warming. Sola 5:164–167

Taylor KE, Williamson DL, Zwiers FW (2000) The sea surface temperature and sea-ice concentration boundary conditions for AMIP II simulations. PCMDI Report 60, Program for Climate Model Diagnosis and Intercomparison, Lawrence Livermore National Laboratory

Vecchi GA, Soden BJ (2007) Increased tropical Atlantic wind shear in model projections of global warming. Geophys Res Lett. https://doi.org/10.1029/2006gl028905

Voldoire A et al (2013) The CNRM-CM5. 1 global climate model: description and basic evaluation. Clim Dyn 40:2091–2121

Voldoire A, Saint-Martin D, Sénési S, Decharme B, Alias A, Chevallier M, Colin J, Guérémy J-F, Michou M, Moine M-P, Nabat P, Roehrig R, Salas y Mélia D, Séférian R, Valcke S, Beau I, Belamari S, Berthet S, Cassou C, Cattiaux J, Deshayes J, Douville H, Franchisteguy L, Ethé C, Geoffroy O, Lévy C, Madec G, Meurdesoif Y, Msadek R, Ribes A, Sanchez E, Terray L (2019) Evaluation of CMIP6 DECK experiments with CNRM-CM6-1. J Adv Model Earth Syst. https://doi.org/10.1029/2019MS001683

Walsh KJE, Fiorino M, Landsea CW, McInnes KL (2007) Objectively determined resolution-dependent threshold criteria for the detection of tropical cyclones in climate models and reanalyses. J Clim 20:2307–2314

Walsh KJE, McBride JL, Klotzbach PJ, Balachandran S, Camargo SJ, Holland G, Knutson TR, Kossin JP, Lee T-C, Sobel A, Sugi M (2016) Tropical cyclones and climate change. WIREs 7(1):65–89. https://doi.org/10.1002/wcc.371

World Meteorological Organization (2014) Atlas of mortality and economic losses from weather, climate and water extremes. WMO no 1123

Yamada Y, Oouchi K, Satoh M, Tomita H, Yanase W (2010) Projection of changes in tropical cyclone activity and cloud height due to greenhouse warming: global cloud-system-resolving approach. Geophys Res Lett 37:L07709

Yessad K, Bénard P (1996) Introduction of local mapping factor in the spectral part of Météo-France global variable mesh numerical forecast model. Q J R Meteorol Soc 122:1701–1719

Zarzycki CM (2016) Tropical cyclone intensity errors associated with lack of two-way ocean coupling in high-resolution global simulations. J Clim 29(23):8589–8610. https://doi.org/10.1175/JCLI-D-16-0273.1

Zhao M, Held IM, Lin SJ, Vecchi GA (2009) Simulations of global hurricane climatology, interannual variability, and response to global warming using a 50-km resolution GCM. J Clim 22:6653–6678